ANL-76-22

ANL-76-22

INL Technical Library

241034

PLEASE RETURN TO
MFC BRANCH LIBRARY

MATERIALS SCIENCE DIVISION
COAL TECHNOLOGY
FIFTH QUARTERLY REPORT,

OCTOBER–DECEMBER 1975

RETURN TO REFERENCE FILE
TECHNICAL PUBLICATIONS
DEPARTMENT

U of C-AUA-USERDA

ARGONNE NATIONAL LABORATORY, ARGONNE, ILLINOIS

Prepared for the U. S. ENERGY RESEARCH
AND DEVELOPMENT ADMINISTRATION
under Contract W-31-109-Eng-38

The facilities of Argonne National Laboratory are owned by the United States Government. Under the terms of a contract (W-31-109-Eng-38) between the U. S. Energy Research and Development Administration, Argonne Universities Association and The University of Chicago, the University employs the staff and operates the Laboratory in accordance with policies and programs formulated, approved and reviewed by the Association.

MEMBERS OF ARGONNE UNIVERSITIES ASSOCIATION

The University of Arizona
Carnegie-Mellon University
Case Western Reserve University
The University of Chicago
University of Cincinnati
Illinois Institute of Technology
University of Illinois
Indiana University
Iowa State University
The University of Iowa
Kansas State University
The University of Kansas
Loyola University
Marquette University
Michigan State University
The University of Michigan
University of Minnesota
University of Missouri
Northwestern University
University of Notre Dame
The Ohio State University
Ohio University
The Pennsylvania State University
Purdue University
Saint Louis University
Southern Illinois University
The University of Texas at Austin
Washington University
Wayne State University
The University of Wisconsin

NOTICE

This report was prepared as an account of work sponsored by the United States Government. Neither the United States nor the United States Energy Research and Development Administration, nor any of their employees, nor any of their contractors, subcontractors, or their employees, makes any warranty, express or implied, or assumes any legal liability or responsibility for the accuracy, completeness or usefulness of any information, apparatus, product or process disclosed, or represents that its use would not infringe privately-owned rights. Mention of commercial products, their manufacturers, or their suppliers in this publication does not imply or connote approval or disapproval of the product by Argonne National Laboratory or the U. S. Energy Research and Development Administration.

Printed in the United States of America
Available from
National Technical Information Service
U. S. Department of Commerce
5285 Port Royal Road
Springfield, Virginia 22161
Price: Printed Copy $4.50; Microfiche $2.25

Distribution Category:
Coal Conversion and Utilization—
Materials and Components (UC-90h)

ANL-76-22

ARGONNE NATIONAL LABORATORY
9700 South Cass Avenue
Argonne, Illinois 60439

MATERIALS SCIENCE DIVISION
COAL TECHNOLOGY FIFTH QUARTERLY REPORT, OCTOBER—DECEMBER 1975

Person in Charge:

R. W. Weeks
Associate Division Director

TABLE OF CONTENTS

LIST OF FIGURES

LIST OF FIGURES (Contd.)

LIST OF TABLES

MATERIALS SCIENCE DIVISION
COAL TECHNOLOGY FIFTH QUARTERLY REPORT,
OCTOBER-DECEMBER 1975

HIGHLIGHTS

Task A -- Evaluation of Ceramic Refractories for Slagging Gasifiers (R. Swaroop)

The 1200-h exposure slag-corrosion cup test using acidic slag was completed. The experimental results indicate that attack by acidic slag was less severe than observed for the basic slag. The first (201 h) test using the slag-abrasion-corrosion rig was completed with some problems. The North Dakota lignite slag that contained ∿13% lime was used in this run. The circumferential specimens experienced a total of 201 h of slag corrosive action with only 70 h of rotational (abrasive) action. A few refractories indicated fairly good corrosion and abrasion resistance to slag attack under the experimental conditions.

Task B -- Evaluation of Ceramic Coatings for Coal-conversion Plants (R. Swaroop)

Progress in this program was made in the (1) preparation of coated specimens for erosion testing at Solar, Inc., (2) corrosion testing of coated specimens for 100- and 500-h exposures, and (3) preparation of a literature survey on the state of the art of the various coating systems.

Task C -- Nondestructive Testing of Coal-plant Components (W. A. Ellingson)

Field tests performed on the CO_2 Acceptor recycle gas heater in Rapid City, South Dakota using infrared scanning revealed that the surface temperature variation of the tubes did not exceed 1% at 980°C. This indicates a uniform flow through the tube bundle. A similar inspection of the expansion-joint bellows yielded a maximum temperature difference of 3°C.

An in-service inspection was performed on the lining of the HYGAS cyclone separator. The accumulated ultrasonic wall-thickness data will serve as a base line for future measurements to determine erosion rates.

Various stud-welding techniques were evaluated to select a method for attaching ultrasonic delay lines to existing piping in coal-gasification plants. The selected method will be applied to equip the 90° bent pipe section for the Synthane plant with wave guides. The instrumented bent section is being manufactured. At the same time, the reliability of ultrasonic wall-thickness measurements at elevated temperature is being assessed. Acoustic-emission technology is being evaluated for application as a leak-detection method for valves. Preliminary results with various orifices for leak-rate calibration are encouraging.

Task D -- Corrosion Behavior of Materials in Coal-conversion Processes
(K. Natesan and O. K. Chopra)

The carburization behavior of Inconel 600 and 625, Incoloy 800, and Type 310 stainless steel has been evaluated by exposing sheet specimens of these alloys to a CH_4-H_2 gas environment for periods of 100, 500, and 1000 h at 875°C. Data show that the values for carbon gain obtained by combustion analyses are in excellent agreement with the measured weight change for all the alloys. The results also show that, at a given carbon activity, the extent of carburization increases with an increase in the chromium content of the alloy.

Task E -- Erosion Behavior of Materials in Coal-conversion Processes
(M. M. Mamoun)

The analytical models developed for determining material loss by erosion have been extended to take into account the effect of mass flow rate of the erosive media. The models have been used to predict erosion rates, as a function of the impact velocity, of a ductile metal and a brittle

nonmetallic surface for which experimental data exist. In the case of a high-purity alumina surface, the predicted velocity dependence of the weight loss was in good agreement with the experimental data. However, the calculated erosion rates for both types of material were a factor of ∿2 to 3 times greater than the experimental data under conditions in which all of the incoming particles were assumed to impact the surface. Since only a fraction of the particles that constitute the erosive media impact the surface, because of collisions with the rebounding particles, the predicted erosion rates were only slightly larger than the experimental values. Additional experimental data are required to further establish the validity of the erosion models, which can then be used to optimize the materials and the design of components in coal-conversion plants.

Task F -- Component Performance and Failure Analysis (S. Greenberg, D. R. (Diercks, W. A. Ellingson, A. Purohit, J. E. Sanecki, W. J. Shack, and J. Y. N. Wang)

1. HYGAS Pilot Plant

An abbreviated version of the final report on instrument tubing failure has been distributed. Incoloy 800 tubes used to replace the original Types 304 and 316 stainless steel tubes, in accordance with our recommendation, continue to operate satisfactorily. Stress analysis of the failed coal pretreatment vessel cooler indicated that failure was caused by plastic buckling, which probably resulted from excessive cooling of the failed pipe. The start-up burner expansion-joint bellows failed as a result of extensive melting. There was no evidence of coal products in the bellows.

2. Synthane Pilot Plant

Acceptable methods of field checking the alloy steel process-piping system were agreed upon, and repair of the system has been completed. Investigation of the failed coal-bucket elevator was terminated when it was

learned that the appropriate components were not available for examination. Failure of the stainless steel elbow-flange welded assembly was diagnosed as primarily the result of poor welding technique. In addition, the elbow appeared to be severely stress-corrosion cracked, probably as the result of chlorides introduced with the pressure testing fluid.

MATERIALS SCIENCE DIVISION
COAL TECHNOLOGY FIFTH QUARTERLY REPORT,
OCTOBER—DECEMBER 1975

ABSTRACT

Results on refractories tested in the slag-corrosion-cup test indicate that attack by acidic slag is less severe than by basic slag. The first (200 h) test in the ANL slag-abrasion-corrosion test rig was completed. Nondestructive tests have been conducted by ANL at the CO_2 Acceptor plant and the HYGAS plant, and an instrumented piping section is being prepared for the Synthane plant. Carburization studies, which have been performed on several alloys, indicate that the extent of carburization increases with an increase in the chromium content of the alloy. Present erosion models predict greater erosion rates than found experimentally, but they assume all particles impact the surface. Failure analyses have been conducted for HYGAS materials, and support in materials identification was given to Synthane plant personnel.

Introduction

The present work is being performed by Argonne National Laboratory (ANL) for the Fossil Energy Division of ERDA. This is the fifth quarterly report on the six major tasks:

A. Evaluation of ceramic refractories to withstand abrasion-corrosion by coal slag that will be encountered in the Bituminous Coal Research (BCR) Bi-Gas coal-gasification pilot plant;

B. Evaluation of ceramic coatings and refractories for metal parts to increase their resistance to erosion and corrosion in coal-gasification pilot plants;

C. Development, evaluation, and application of nondestructive testing (NDT) methods for use in coal-plant fabrication, construction, and operation to ensure component integrity;

D. Development of computer models to predict the corrosion behavior of materials used in coal-gasification plants;

E. Development of computer models to predict the erosion behavior of materials used in coal-gasification plants; and

F. Analysis of pilot-plant components that have failed or are removed from service for other reasons.

Progress in each of the six tasks is reported in the sections that follow. The work officially began in October 1974. This is the fifth quarterly report, for the period from October through December 1975.

Task A -- Evaluation of Ceramic Refractories for Slagging Gasifiers
(Principal Investigator: R. Swaroop)

1. Slag-corrosion Cup Test

As described in the previous quarterly reports,[1-3] the purpose of this test is to determine the extent of slag penetration and chemical attack of ceramic refractories at high temperatures in an oxygen-steam environment. The experimental conditions of this test partially simulate the operating environment of the first stage of the Bi-Gas gasifier.

The 1200-h-exposure slag-corrosion cup test using acidic slag was completed. The composition of the acidic slag used in this test was reported earlier.[3] The base-to-acid ratio of the acidic slag varies between 0.71 and 0.73, and the melting range is between 1400 and 1450°C. The experiments were conducted at ∿1545°C in an oxygen-steam environment. Altogether, 20 refractories were exposed to the acidic slag. The refractories that survived 750 h (or more) of exposure to basic slag were selected for acidic slag exposure. Refractories that were received from companies during or after the last run for basic-slag exposure were also included in the acidic-slag exposure test. The compositions of the refractories were reported previously,[3] except for refractories 24 through 27. The compositions of these refractories are listed in Table I.

TABLE I. Composition (wt%) of New Refractories

Refractory Identification Number	Al_2O_3	Fe_2O_3	SiO_2	CaO	$K_2O + Na_2O$	Cr_2O_3	Other
24 (B)	97.6	<0.1	<0.1	1.5	0.4	-	0.2
25 (B)	99.5	0.09	0.07	-	0.25	-	0.4
26 (B)	67.5	-	-	-	-	32.0	0.5
27 (Ramming Mix)	89.7	0.1	0.1	T[a]	0.1	10.0	-

[a] T = trace.

Tables II-IV summarize the observed results from slag-cup tests using acidic slag. In the 1200-h continuous test, the cups were charged with slag initially and then at ∿250, 500, 700, and 850 h. Table II shows the results observed for the specimens exposed for these times and for 1200 h. All 20 refractories except one (36) have survived a 1200-h exposure without severe swelling or development of cracks. Testing of refractory 36 was terminated after 500 h of exposure as the SiC content of the refractory appeared to have reacted with the oxygen-steam environment and formed blisters (molten SiO_2) all over the surface. The additional exposure of refractories 25-27 and 201C was not conducted because of the termination of the slag-cup test. Table III lists the observed dimensional and weight change of the refractory cups. The minimum dimensional change was observed for fusion-cast refractories (2, 4, and 22); however, refractory 22 indicated slight shrinkage or loss of material in the gaseous environment (probably as a result of chromia evaporation). Similarly, phosphate-bonded refractory 201C indicated shrinkage as a result of loss of material. The maximum dimensional change was observed in the case of the magnesia-chromia refractories (18-21), and the next greatest change was in the calcium aluminate-bonded alumina-grain refractory (7).

Table IV compares the results obtained from the acidic and basic slag-cup tests on the basis of grain-bond systems. It is indicated that the effects of the acidic slag were not as severe to the refractories as the basic slag. If a refractory has survived a 1000-h exposure in a basic slag, it appears that it should also have a good compatibility with acidic slag.

2. Slag-abrasion-corrosion Test Rig

As reported earlier,[1-3] the slag-abrasion-corrosion test rig has been constructed to determine the resistance of refractories to the

TABLE II. Slag-corrosion Cup Tests (with Acidic Slag)[a]

Refractory Identification Number[b]		Specimen Condition after				
		250 h	500 h	700 h	850 h	1200 h
2	(B)	P,St	P,St	P,St	P,St	P,St
4	(B)	P,St	P, S(t)	P,St	P,St	P,St
7	(CA)	P	P	P,S	P,S,E	P,E,S
8	(CA)	P, S(S), C(S)	P,E	P,E, Cr(S)	P,E, Cr(S)	P,E
11	(B)	P	P	P	P	P
12	(B)	P	P	P,E	P,E	P,E
15	(B)	P	P	P,Sh	P	-
16	(B)	P	P	P	P	P
18	(CA)	P,C,St,S	P,C,R,S	P,R,C(S)	P,R,Sh,C	P,R,Sh,C,T
19	(B)	P,St	P, C(S)	P, S(S)	P, S(S)	P,R, S(S)
20	(B)	P	P	P, S(S), Cr(S)	P, S(S)	P, S(S)
21	(B)	P	P,R	P,R, S(S)	P,R,S,Cr	P, S(S)
22	(B)	P,St	P,R	P,R	P,St,R	P,St,R
23	(B)	P	P	P, S(S)	P, S(S)	P, S(S)
24	(B)	P,St	P	P	P	P
25	(B)	P	P	-	P	-
26	(B)	P	P	P	-	-
27	(CA)	P,E, S(S)	P,E, S(S), C(S)	P,E, S(S)	-	-
36	(B)	P, E(S), Bi,R	P,R,Bi,T	-	-	-
201C	(CA)	P	P,Sh	-	P,Sh	-

[a] At ~1545°C.

[b] Compositions of refractories should be obtained from Ref. 3.

Bi = blistered.
(B) = brick or preshaped.
C = visible cracks.
(CA) = castable.
Cr = crumbling.
E = etched or eaten away inside the cup.
NA = not available.
P = visible penetration or chemical attack.
R = gaseous reaction with outside obvious (sometimes subliming obvious).
S = swollen.
Sh = slight shrinkage.
St = slag sticks to refractory (sometimes slag overflow welds the lid to cup).
(S) = slight.
T = terminated.

TABLE III. Quantitative Results from the Slag-corrosion Cup Test (using Acidic Slag)[a]

Refractory Identification Number		Range of Exposed Hours	Average wt% Change in Cup plus Lid	Average Dimensional Change in Cup, %		Remarks
				Top	Bottom	
2	(B)	0-1203	3.4	1	0	
4	(B)	0-1203	5.0	0	1	
7	(C)	0-1203	18.3	9.7	6.2	
8	(C)	0-1203	-0.10	1.7	3.4	
11	(B)	0-1203	-1.7	1.5	2.1	
12	(B)	0-1203	7.3	4.0	3.4	
15	(B)	0-943	7.3	2.8	3.7	
16	(B)	0-1203	9.1	2.8	2.3	
18	(C)	0-1203	1	NA[b]	NA	Could not measure.
19	(B)	0-1203	-1.3	10.8	10.2	
20	(B)	0-1203	-0.3	10.0	11.9	
21	(B)	0-1203	15.2	9.7	10.1	
22	(B)	0-1203	-14.8	-3.8	-4.5	
23	(B)	0-1203	12.2	2.5	3.0	
24	(B)	0-1203	2.4	0	0.9	
25	(B)	0-943	6.9	0	2.1	
26	(B)	0-690	8.6	0.5	1.0	
27	(C)	0-690	4.2	1.5	2.3	
36	(B)	0-513	-11	NA	NA	Reacted badly with O_2-H_2O environment.
201C	(C)	0-943	-18.5	-2.6	-2.9	

[a]Composition of refractories can be obtained from Ref. 3.

[b]NA = not available.

TABLE IV. Cup-slag-corrosion Test Results

Refractories	Grain-bond System	Number of Hours[a] Survived		Remarks
		Basic Slag	Acidic Slag	
7,8,9	Tabular Al_2O_3-Calcium Aluminate (92-96%)-(4-6%)	250-500	1000	Reacted severely with acidic[b] slag after 500 h.
12-15	Tabular Al_2O_3-Mullite (90-92%)-(7-11%)	250-750	1000	Best results were from 12.
6,10,11,17	Tabular Al_2O_3-Phosphate (84-95%)-(1-5%)	250-750	1000	Best results were from 17. Only refractory 11 was exposed to acidic slag.
18 (Ramming Mix)	Chrome/Al_2O_3-Phosphate (40/22)-(4%)	1000	750-1000	Reacted with acidic as well as basic slag; bond crumbled at ~700 h.
2,4	Fusion-cast Al_2O_3 (99%)	1000	1000	Refractory 2 indicated slight swelling after 750 h.
22	Fusion-cast Chrome (80%)	1000	1000	-
16,23,27 (27 Is Ramming Mix)	Alumina-Chromia (90%)-(10%)	1000	1000	Refractory 27 tested in acidic slag up to 700 h only.
19-21	Magnesia-Chromia (52-64%)-(14-20%)	1000	1000	-
1,24,25	Al_2O_3-Sintered (97-99%)	250-500[c]	1000[d]	-

[a]Before developing cracks, swelling, and disintegration. Test terminated at 1000 h.

[b]On the basis of refractory 8 only.

[c]On the basis of refractory 1 only.

[d]On the basis of refractories 24 and 25 only.

simultaneous abrasive and corrosive attack by slag in simulated environments. Photographs of this rig were shown earlier.[2,3]

The hookup of all utilities was completed on Oct. 15, 1975. The safety test runs for these utilities, including the CO/CO_2 system, were completed and approved by the Materials Science Division/ANL Safety Committee on Nov. 20, 1975. The initial curing of the rig was completed by Dec. 10, 1975, and the maiden run with 15 different refractories using slag obtained from North Dakota Lignite Coal was begun on Dec. 12, 1975. The refractories were chosen principally from those that exhibited good performance in the cup tests.

Experiment: The first 200-h test was completed on Dec. 19, 1975. However, some problems were encountered: (a) failure of the electronic circuit of the drive system for the center shaft, (b) burnout of one of the Pt-thermocouples, and (c) difficulties in pouring out the slag after the run was completed. Problem (a) caused the refractories to undergo one extra thermal cycle (1500→500→1500°C) over a 24-h period. The drive motor was replaced by an air-driven motor. Problem (c) caused the specimens to undergo another thermal cycle (1500→300→1500°C). Another major problem that deals with the center shaft came to our attention after the initial run was completed. Sometime between 61 and 109 h of rotational time, the bottom cylinder, which contained eight rotational specimens (R-specimens), fell apart as a result of thermal cracks developed earlier. Hence, the R-specimens were sitting in the slag for between 61 and 109 h. The abrasive action on the stationary specimens located along the circumference of the rig (C-specimens) that was caused by the rotation of the center shaft was therefore absent sometime after 61 h. A more careful examination of the data reveals that at least a 70-h rotational (abrasive) effect and a total of 201 h of

corrosive action were achieved on the C-specimens during this run. The other experimental conditions during this run are listed in Table V. The rotational speed of the center shaft was ∿10 rpm. This produced a calculated slag drag of 30.5 cm/min on the R-specimens and 5.1 cm/min on the C-specimens. This calculation was based upon the Newtonian motion in the slag.

TABLE V. Experimental Conditions during Slag-abrasion-corrosion Test Run 1

Conditions	Details
$CO-CO_2$ Ratio	CO/CO_2 = 1.5; partial pressure of O_2 $\sim 10^{-8}$ atm[a]
Flow Rate	($CO + CO_2$) flow rate = 4 liters/min. Linear flow rate at the nozzle = 8.4 m/s (27.6 ft/s)
Temperature of Slag	1450-1500°C
Time of Exposure	201 h of corrosive action on the C-specimens plus at least 70 h of abrasive action on the C-specimens and center-shaft specimens
Thermal Cycles	4 (on the C-specimens)
Rotational Speed	10 rpm

[a]Chemical analysis of exhaust gases indicated $P_{O_2} \approx 10^{-7}$.

Results:

(a) Table VI lists the observed results from the 15 refractories. These data are reported in terms of the maximum abraded (or eroded) depth of the refractory and the normalized material loss. This table also lists the maximum depth of visible slag penetration into the refractory. The minimum and maximum material loss was observed in refractories 22 and 7, respectively. The grain-bond systems were identified in Table IV. The refractories that indicated fairly good corrosive and abrasive resistance to the slag are: 4, 12, 15-17, and 19-22. Refractories 4, 14, 18, and 22 developed cracks

TABLE VI. Refractory Material Loss during Slag-abrasion-corrosion Test Run 1

Refractory Identification Number[a]		Material Abraded,[b] vol %	Maximum Depth of Abrasion, mm	Maximum Depth of Visible Slag Penetration, mm	Remarks
1	(B)	6.4	16	33	-
4	(B)	0.65	2.8	<1	One small crack after curing. Developed transverse and longitudinal cracks during run.
7	(CA)	22.2	26.7	51	Severely reacted and disintegrated.
8	(CA)	21.4	23.5	33	Severely reacted and disintegrated.
10	(CA)	7.1	18.8	30	-
12	(B)	3.0	10.0	<2	-
14	(B)	2.65	11.7	8	Developed a feeble transverse crack during run.
15	(B)	1.86	6.9	5	-
16	(B)	1.1	5.3	15	Developed small cracks during run.
17	(B)	1.9	7.4	18	-
18	(CA)	21.35	21.1	c	Developed cracks while curing, i.e., before slag was molten.
19	(B)	2.65	7.9	13	-
20	(B)	2.56	6.9	13	-
21	(B)	1.58	7.4	15	-
22	(B)	≈0	≈0	ND[d]	Developed side-to-side cracks during run; no obvious corrosive or abrasive actions.

[a]For grain-bond system, refer to Table IV.

[b]Normalized.

[c]Difficult to measure even though slag penetration was obvious.

[d]ND = not detectable.

during the run. The development of cracks in fusion-cast dense refractories (4, 22) due to the thermal cycling was expected. Refractories 7 and 8, which are castable refractories, disintegrated badly and indicated a large materials loss during the run.

Figure 1 shows a comparison of the conditions of the four C-specimens before and after the test. The disintegration of refractory 18 by the abrasive and corrosive action of the slag is apparent (Fig. 1c). The abrasion-corrosion line of slag on the refractories is distinct.

(b) The slag used in this run was sent by Minnekota Power Corp., North Dakota, and was reported to have been obtained from burning North Dakota lignite coal. Even though the slag contains 13% CaO (Table VII), the analyzed base-to-acid (B/A) ratio was <1 (i.e., $\approx$0.49). This was supposed to be a basic slag; however, the high content of silica causes it to be acidic. The B/A ratio of the slag changed from 0.49 to 0.40 over a period of 201 h. This slight change occurred as a result of dissolution of Al_2O_3 from the refractories. The Al_2O_3 content changed from 17 to 26% over this period. Therefore, the nature and composition of the slag practically remained the same during the run.

3. Future Work

The future effort in this program will be as follows:

a. The failed and unfailed refractory specimens exposed to acidic slag in the cup tests will be analyzed to determine the failure mechanisms and identify any newly formed product(s). This is a continuing effort between ANL and the refractory suppliers.

b. The slag-abrasion-corrosion test rig will be prepared for the second run. This run will probably be conducted with basic slag.

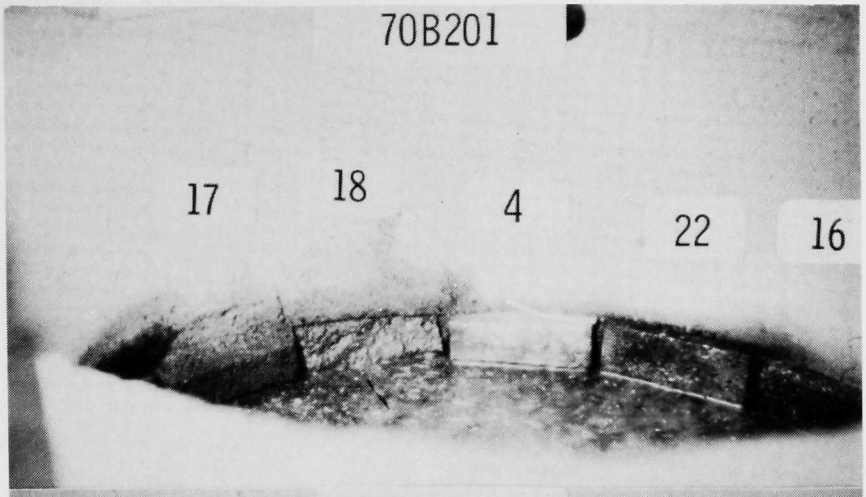

(a) Before

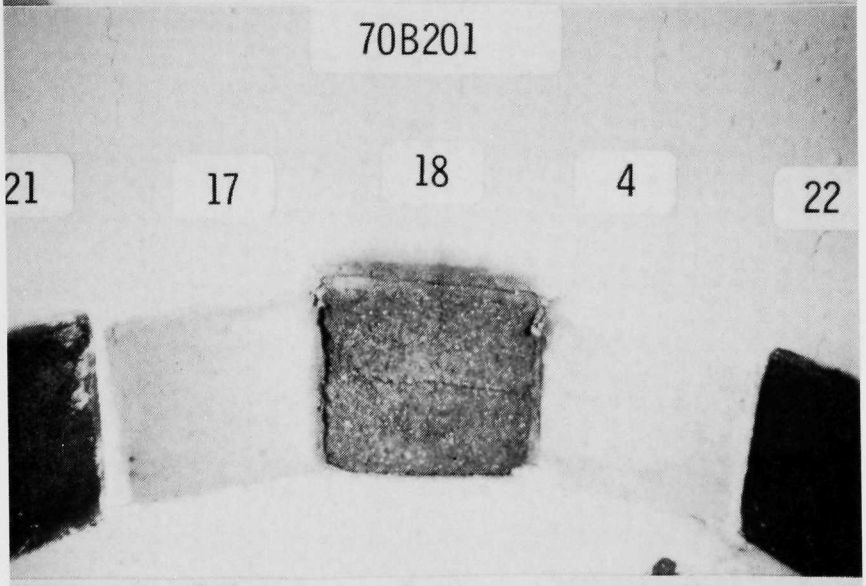

(b) After

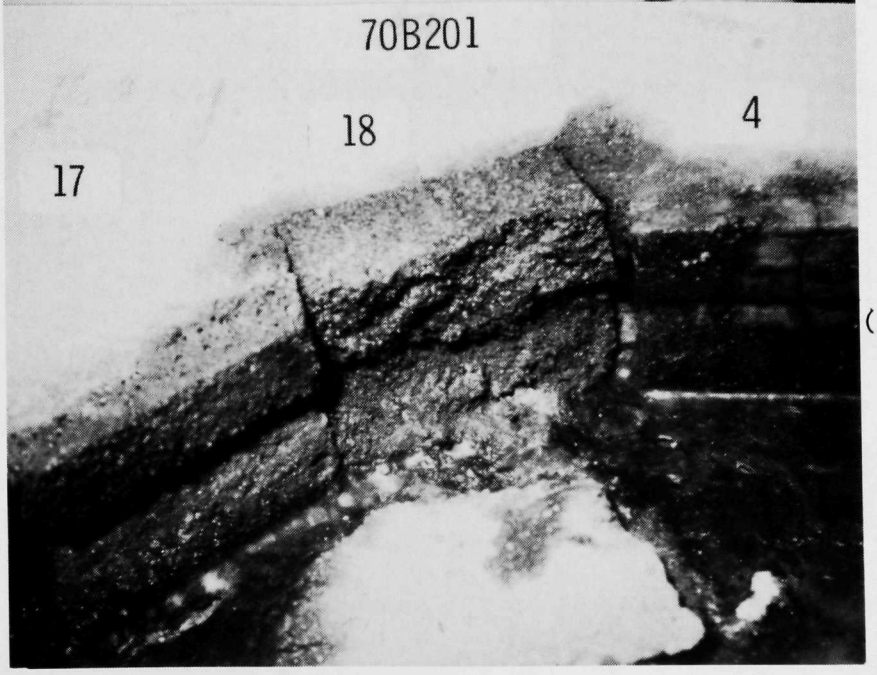

(c) After

Fig. 1. Refractory Specimens before and after Exposure in the Slag-abrasion-corrosion Rig.

TABLE VII. Slag Composition during Abrasion-corrosion Test Run 1

Oxide		Exposure Time,[a] h						
		0 (0)	35 (0)	41 (6)	55 (20)	99 (61)	145 (61)	201 (109)[b]
Al_2O_3	(A)	17.2	18.4	23.0	24.0	24.9	27.2	26.1
SiO_2	(S)	50.2	47.8	46.8	46.0	43.2	43.7	47.2
TiO_2	(T)	0.8	0.7	0.7	0.8	0.75	0.75	0.7
CaO	(C)	13.2	12.5	12.5	12.2	12.8	13.4	13.0
MgO	(M)	4.8	4.3	4.8	4.7	3.9	4.2	3.9
$K_2O + Na_2O$	(N+K)	3-6	4-7	3-6	3-6	3-6	3-6	2-4
Fe_2O_3	(F)	11.0	10.6	9.5	9.7	8.7	8.4	8.1
SO_3	-	0.02	0.02	0.01	0.01	0.01	<0.01	<0.01
P_2O_5	(P)	0.10	0.21	0.09	0.09	0.08	0.07	0.07
V_2O_5	(V)	0.05	0.06	0.05	0.04	0.04	0.04	0.04
B/A Ratio[c]		0.49	0.49	0.45	0.44	0.46	0.44	0.40

[a]The numbers in parentheses refer to the total shaft rotational time.

[b]Abrasive action on C-specimens would be minimal because rotating shaft bottom disintegrated between 61 and 109 h.

[c]B/A = (F + C + M + N + K)/(S + A + T).

Task B -- Evaluation of Ceramic Coatings for Coal-conversion Plants
(Principal Investigator: R. Swaroop)

The ceramic coatings program has progressed in the following areas during the past three months: (1) preparation of coatings using the plasma-spray technique, (2) exposure of coated specimens to a coal-gas mixture for 100 and 500 h, (3) preparation of a literature survey on the state of the art of the various coating systems and coating manufacturing technologies, and (4) the design and construction of a 1-atm corrosion-erosion test rig at Solar, Inc. on subcontract.

1. Preparation of Coatings

(a) Plasma-spray coatings (≈250 μm thick) of various oxides (Table VIII) were prepared over substrates of Types 304 and 310 stainless steel and Incoloy 800. These coatings had composite three-layer structures. The first layer on the substrate consisted of a metal or alloy matrix (Ni-Al or Ni-Cr type), the second layer was a mixture of alloy with 50% ceramic compound (Al_2O_3, MgO, or ZrO_2), and the top layer consisted of 100% ceramic compound. This three-layer structure has been prepared to reduce thermal mismatch between the substrate and coating. Table VIII lists the details of these coatings with the measured hardness of the top layers. These substrate-coating systems will be tested for thermal-shock resistance and then for corrosion resistance in a coal-gas mixture.

(b) The efforts on ion-plated coatings will be deferred until later in the program since the plasma-spray coatings are of higher priority.

2. Corrosion Testing

Various coated substrates were evaluated in a representative coal-gas mixture, such as that produced in the high Btu pilot plants. The average composition of this gaseous mixture has been reported earlier[3] along with testing conditions and the criteria for a coating to resist corrosion.

TABLE VIII. Plasma-spray Three-layer Composite Coatings

Substrate-coating System[a]	Hardness,[b] Rc
1. Substrate - BC[c] - 50% (NiCrAl) + 50% $MgOAl_2O_3$ - $MgOAl_2O_3$	60-65
2. Substrate - BC - 50% (NiCrAl) + 50% Cr_2O_3 - Cr_2O_3	65-68
3. Substrate - BC - 50% (NiCrAl) + 50% $MgOZrO_2$ - $MgOZrO_2$	47-52
4. Substrate - BC - 50% (NiCrAl) + 50% $Al_2O_3Cr_2O_3$ - $Al_2O_3Cr_2O_3$	60-65
5. Substrate - BC - 50% (NiCrAl) + 50% ZrO_2 - ZrO_2	40-50
6. Substrate - BC - 50% (NiCrAl) + 50% Al_2O_3 - Al_2O_3	65-68

[a]Substrates were Types 304 and 310 stainless steel and Incoloy 800.
[b]Of top layer.
[c]BC = bond coat of (NiCr).

Table IX lists the various substrate-coating systems that were corrosion tested during the past three months. It appears that the Co-Cr-Al alloy retards corrosion and protects the substrate up to 100 h; however, this protective capability gradually fails with time. Similar results were obtained for the chromium carbide coatings, as shown in Table IX. The Triboloy 800 material indicated good corrosion protection of Type 310 stainless steel up to 100 h and retarded the corrosion attack of Type 304 stainless steel for the same period. Microscopic examination of corrosion-tested specimens will be conducted and reported later.

3. Literature Survey

A literature survey has been made of the state of the art of various coating systems and their manufacturing techniques as well as the capability of the present coating technologies to produce suitable ceramic coatings for use in coal-gas environments. This survey is presently being internally

TABLE IX. Corrosion Testing of Various Plasma-spray Coating-Substrate Systems (in Coal-Gas Mixture at 980°C)

Substrate-Coating	Hours Exposed	Results	Specimen Identification Number
304 SS - BC - $MgOZrO_2$	100	R, S(one side)	A14T
304 SS - BC - $MgOZrO_2$	500	R	A14T
310 SS - BC - $MgOZrO_2$	100	R, S(on edges)	E14T
304 SS - BC - (Co-Cr-Al) Alloy	100	R(M)	A18T
304 SS - BC - (Co-Cr-Al) Alloy	500	C	A18T
304 SS - BC - ZrO_2	100	R(M)	A12T
310 SS - BC - ZrO_2	100	R	E12T
316 SS - BC - ZrO_2	500	R	B12T
304 SS - BC - Triboloy 800	100	R(M)	A19T
310 SS - BC - Triboloy 800	100	R	E19T
304 SS - BC - Cr_3C_2 (NiAl)	500	R(M)-C[a]	A11T
316 SS - BC - Cr_3C_2 (NiAl)	500	R(M)-C[a]	B11T

[a]Corrosion was retarded up to 100 h of exposure.

BC = bond coat of NiCr alloy.
C = failed to resist corrosion.
R = resisted corrosion.
R(M) = retarded corrosion.
S = spalled during cooling.

reviewed and will be released shortly. Table X lists the recommended manufacturing techniques that should be explored and/or developed to produce appropriate ceramic coatings.

4. Corrosion-Erosion Test at Solar, Inc.

Solar has reported that a wooden mock-up apparatus was constructed to perform a design analysis for particle-impingement at various velocities. This, they felt, was necessary before constructing the corrosion-erosion test rig, which will be built on the basis of the design analysis.

TABLE X. Recommended Manufacturing Techniques for Ceramic Coatings

Technique	Coating Materials	Relative Cost	Present Status
Plasma Spray	Oxides, carbides, nitrides, and borides	Relatively inexpensive	C[a]
Ion Plating	Oxides, carbides, and nitrides	Initial capital expenses for equipment are high	D[b]
Chemical Vapor Deposition	Oxides and carbides	Initial capital expenses for equipment and operational cost are high	D
Vitreous Refractory Coatings	Oxides only	Relatively inexpensive	C

[a] C = commercial.

[b] D = developmental.

Thirty bent specimens of Types 304 and 310 stainless steel and Incoloy 800 were coated with various ceramic coatings (Al_2O_3, Cr_2O_3, $MgOZrO_2$, and ZrO_2) and sent to Solar for testing.

5. Future Work

The future work in this program will deal with (a) evaluation of new bond coats with improved thermal-spalling resistance, (b) preparation of oxide-coated specimens with graded interfaces for Solar, (c) thermal-shock and corrosion testing of new substrate-coating systems, and (d) microscopic evaluation of the exposed specimens.

Task C -- Nondestructive Testing of Coal-plant Components
(Principal Investigator: W. A. Ellingson)

1. Infrared

(a) A field investigation of the CO_2 Acceptor recycle gas heater B-205 in Rapid City, South Dakota was conducted on Oct. 21-24, 1975 to

determine if temperature differentials existed among adjacent tubes in the interlaced five-tube helix. Such a differential would be indicative of differential gas mass flows within the tube complex (Fig. 2). Flue gas from

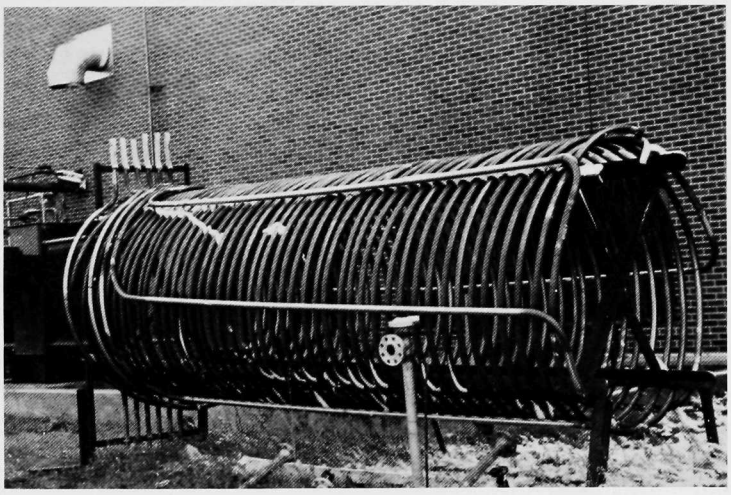

Fig. 2. Helical Interlaced Replacement Tubes Similar to Those in Heater B-205. Neg. No. MSD-62442.

the Acceptor regenerator is fed into the complex of five Inconel 702 tubes (5.08-cm outside diameter x 0.48-cm wall) from a single manifold. A knowledge of the uniformity of the gas mass flow among the five tubes was desired. The gas in the tubes with the higher flow rates has a shorter residence time and hence would not achieve as high a temperature as the gas with the lower flow rates. Thus, the tubes with the higher flow rates and shorter residence times should exhibit cooler outer surface temperatures. Also considered was the possibility that a significantly hotter tube might contribute to premature failure. Previous attempts to measure tube surface temperatures with thermocouples had not been successful because of rapid thermocouple deterioration in the furnace. Since the furnace operates at temperatures above 980°C and the tubes are glowing with a white-heat color at that temperature, it is not possible to visually detect overall thermal gradients. However, infrared imaging can detect these gradients via remote sensing.

An AGA passive infrared scanning camera and front surface mirror were situated under the recycle gas heater (Figs. 3 and 4), and "on-line" viewing of the tubes was achieved through a 10.16 x 15.24-cm inspection port. The five adjacent tubes were scanned. These tubes exhibited a temperature differential of 10°C. This is ∿1% of the operating temperature (Fig. 5). This indicated that no tube was significantly hotter than its neighboring tubes and the gas flow through the tube complex was essentially uniform.

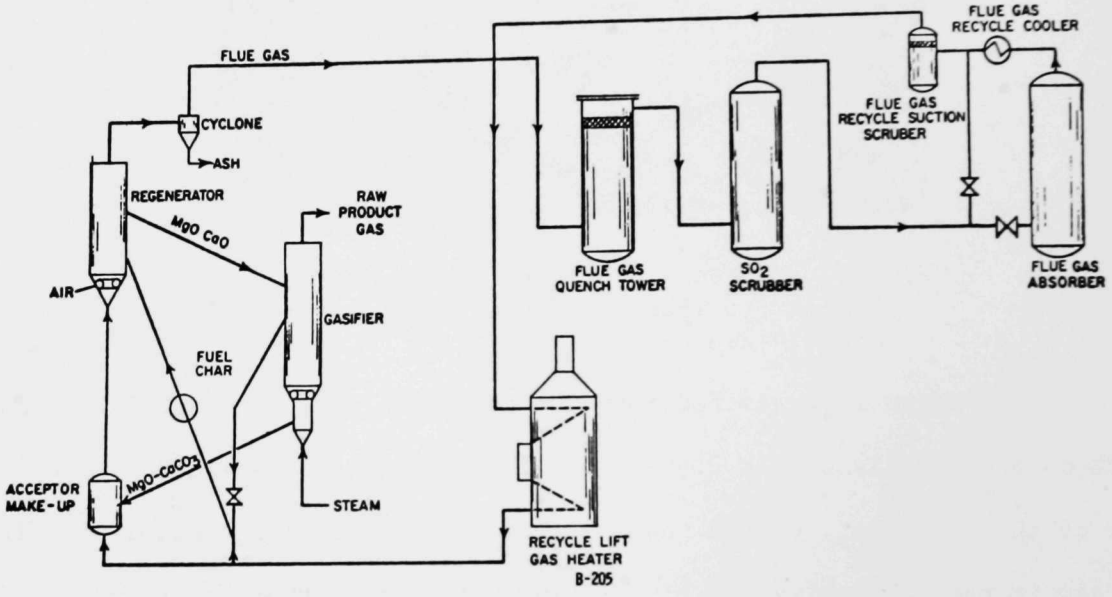

Fig. 3. Flow Diagram of CO_2 Acceptor Process That Relates to Heater B-205. Neg. No. MSD-62438.

A second component investigated for thermal gradients was an Incoloy 825 expansion-joint bellows on the CO_2 spent Acceptor lift line. This was examined to determine if any hot spots existed that might contribute to premature failure. Using the warmest spot (93°C) for the reference temperature, the temperature differential from the warmest to the coolest convolution was measured to be 3°C, with the uppermost convolution (located over the expansion joint) the warmest and the lowest convolution the coolest (Figs. 6-9). No significant thermal gradients were detected.

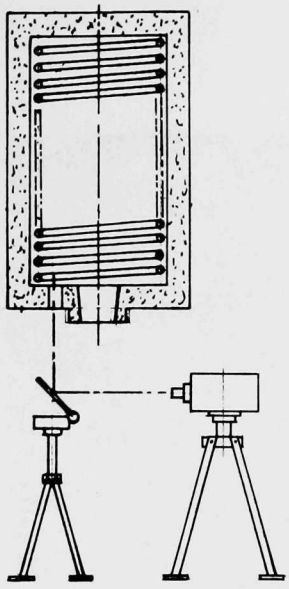

Heater B-205 Nomenclature

Tubes: Inconel 702 (2-in. OD x 3/16-in. Wall)
Helix: 5 Tube Interlaced
Gas: Recycle Gas from Regenerator Flue
Pressure: 300 psig
Flow: 60,000 scfh
Operating Temperature: 1800 °F
Inlet Temperature: 225 °F
Fuel: Natural Gas

Fig. 4. Heater B-205 at CO_2 Acceptor Coal-gasification Plant, Rapid City, South Dakota. Neg. No. MSD-62437.

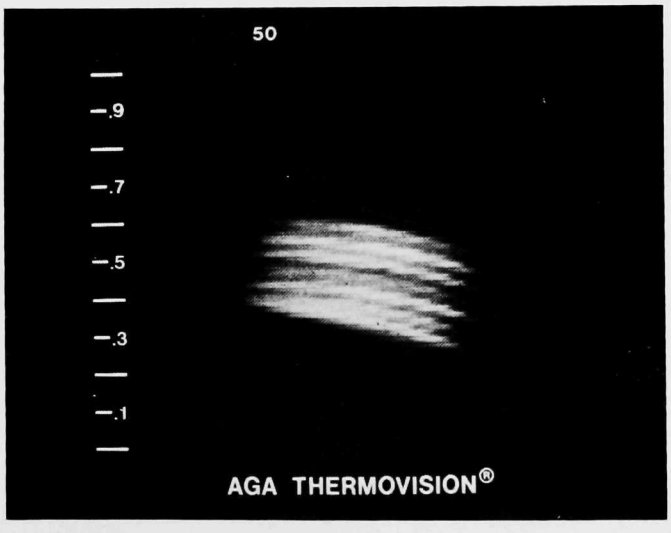

Fig. 5. Analog Infrared Thermogram of Heater Tubes Viewed through the Inspection Port on Heater B-205 at Operating Temperature (4-scan, f-10). Neg. No. MSD-62452.

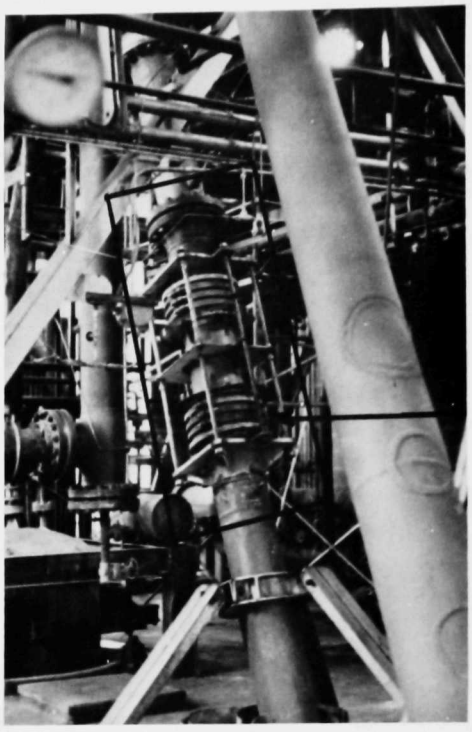

Fig. 6. Spent Acceptor Lift-line Expansion Joint and Bellows. Neg. No. MSD-62443.

Fig. 7. Close-up View of Bellows in Fig. 6. Neg. No. MSD-62444.

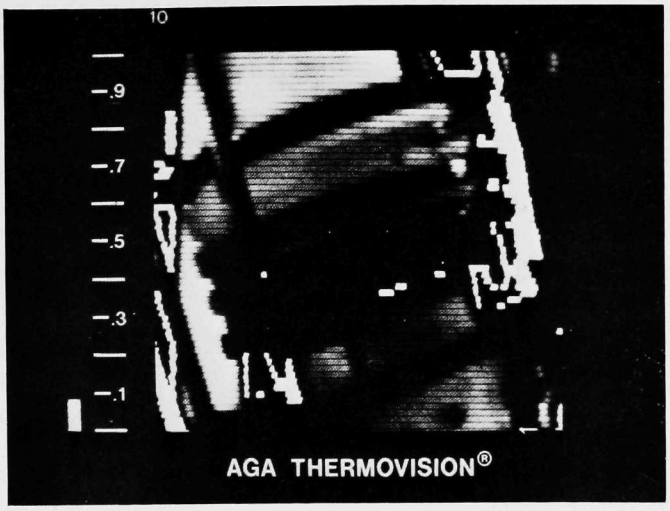

Fig. 8. Infrared Isothermogram of the Warmest Spot on the Coolest Bellows Convolution. Note cursor setting = 0.1 x 10 isotherm units (IU). Reference temperature = 93°C (4-scan, f-205). Neg. No. MSD-62451.

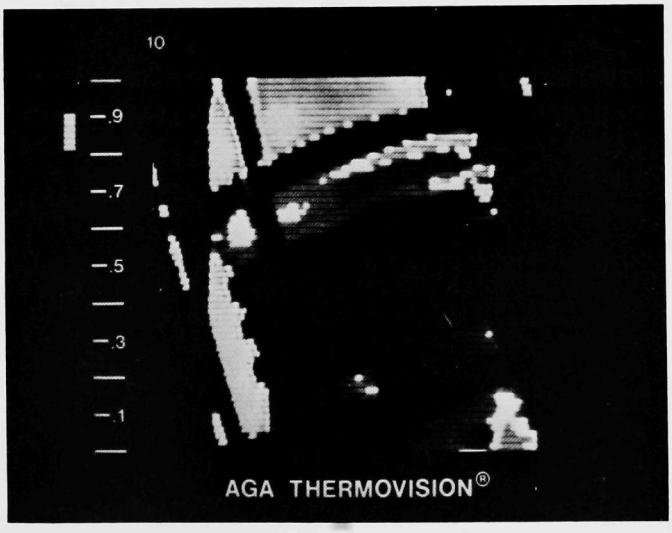

Fig. 9. Same as Fig. 8 but with Isotherm Level Set for Warmest Spot on Warmest Convolution. Note change of cursor level. ΔIU = 0.82 x 10. ΔT = 3°C. Neg. No. MSD-62441.

(b) The 91 x 122 x 61-cm electric test furnace (Fig. 10) has recently been completed, and an 86 x 117-cm cross-section refractory/steel shell laminate mock-up of the Battelle-Columbus gasifier has been cast. A 122 x 122-cm front surface mirror has been ordered for placement over the gasifier mock-up/test furnace to permit infrared scanning of the outer surface of the mock-up at elevated temperatures. After the acoustic-emission test sequence has been completed, artificial defects to represent various degrees of erosion, spalling, and cracking will be generated in the refractory. The mock-up will be heated in the furnace and scanned with the infrared camera from the outer (steel shell) side. The capability of the AGA system to detect defects and gather sufficient data to permit characterization of defects will be assessed.

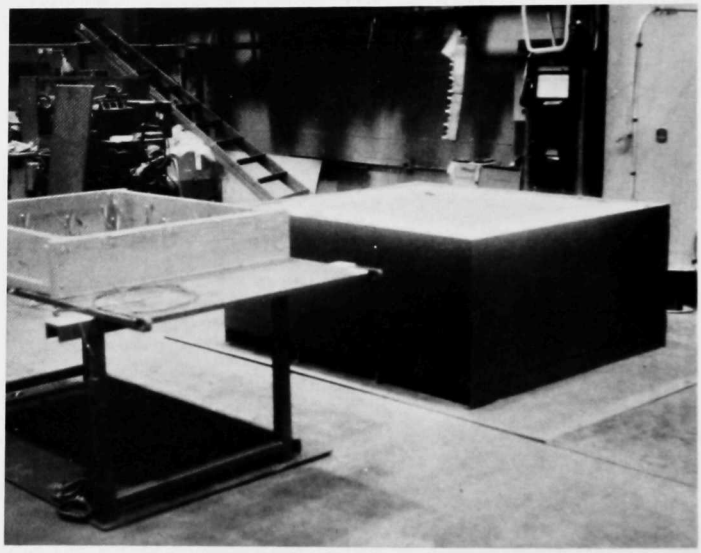

Fig. 10. Electric Furnace on Right for Heating Refractory/Steel Shell Laminate Mock-up. Steel plate with hangers on left is ready for casting with refractory. After casting and drying, the laminate is inverted and placed on top of furnace for heating. Neg. No. MSD-62445.

Future plans include (1) the generation of calibration curves for use with a recently obtained high-temperature filter, (2) a field investigation of the thermal patterns on the surface of the HYGAS gasifier preheater, and (3) conducting a comprehensive infrared scan of the Synthane gasifier during its initial operation. Base-line thermal data generated will be recorded on video tape for later comparison.

2. Ultrasonics

(a) Initial designs and stress calculations have been completed for the completely instrumented replica that will replace a 90° bend section of the Synthane coal-slurry feed line (Fig. 11). The replica, which is to be

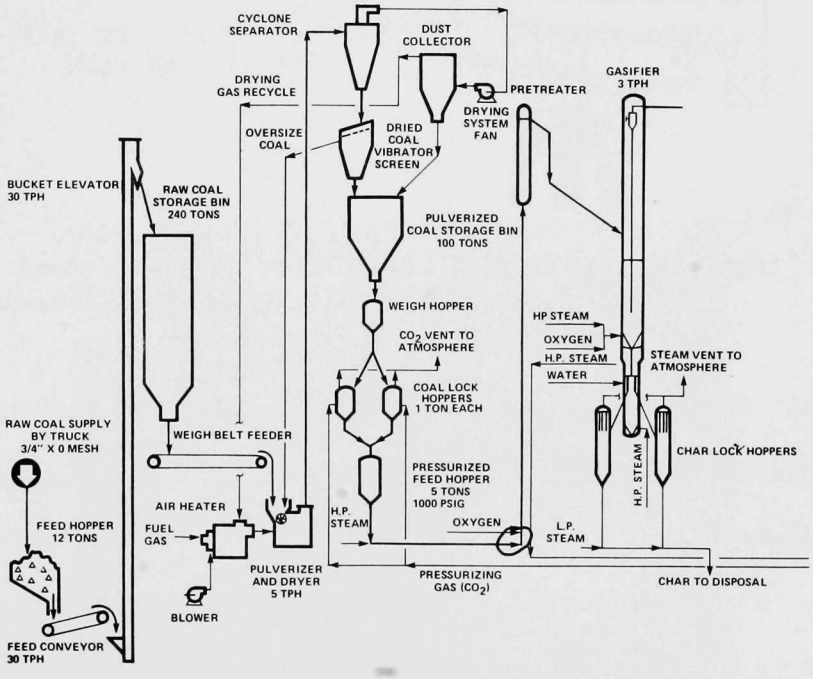

Fig. 11. Flow Diagram of Synthane Process Showing Location of Coal-slurry Feed-line Bend. Neg. No. MSD-62436.

fabricated and hydrostatically tested in the ANL shops, will feature an array of thirty air-cooled ultrasonic waveguides and transducers (Fig. 12). The instrumented replica will be installed in the Synthane system to permit real-time monitoring of pipe-wall thinning in the bend area and mapping of the erosion patterns.

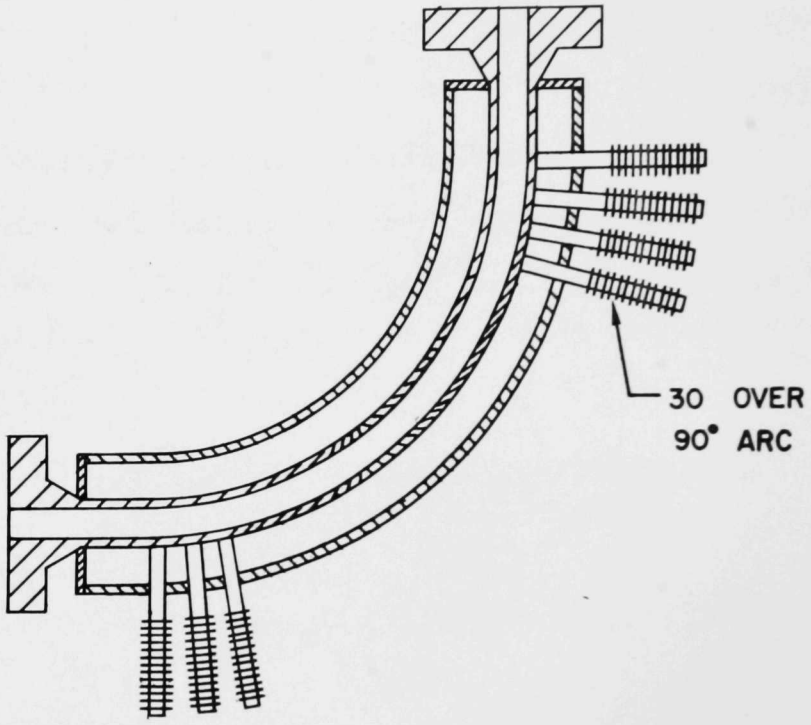

Fig. 12. Replica of Coal-slurry Feed-line Bend with Air-cooled Ultrasonic Delay-line Waveguides. Neg. No. MSD-62428.

(b) An initial study of erosion on the HYGAS high-pressure raw gas cyclone separator was conducted in the laboratory utilizing ultrasonic pulse-echo techniques (Figs. 13-15). The cyclone is a weldment of Type 304 stainless steel. The inner surface of the cyclone in a 180° area where incoming raw gas and particulate matter impinge on the wall contains overlapping weld beads of No. 6 Stellite to provide a hard surface. Thirty-nine points in this area were located with respect to the inlet and mapped in the Stellite-lined region on the outer surface of the cyclone, and twelve points were

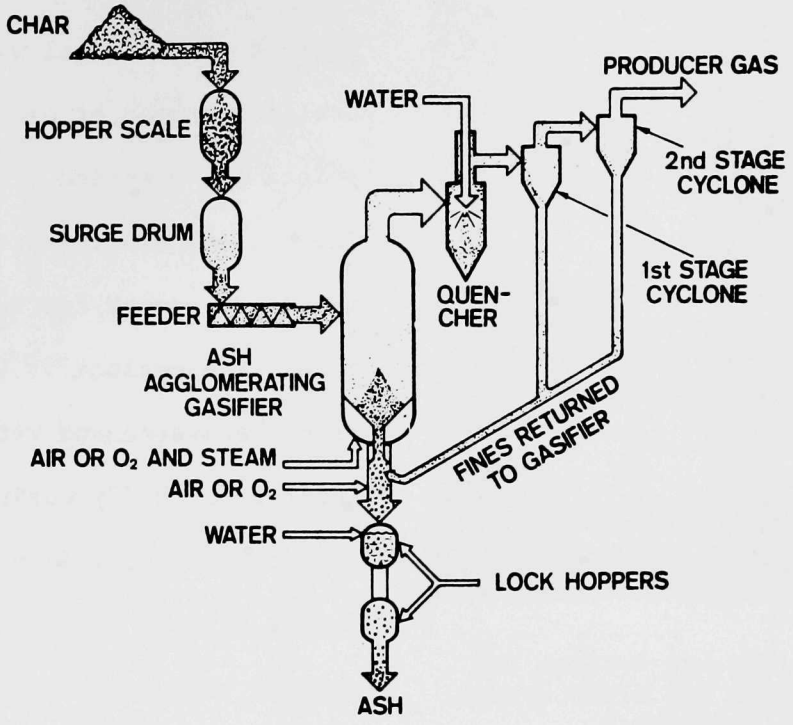

Fig. 13. Flow Diagram of IGT HYGAS Process.
Neg. No. MSD-62435.

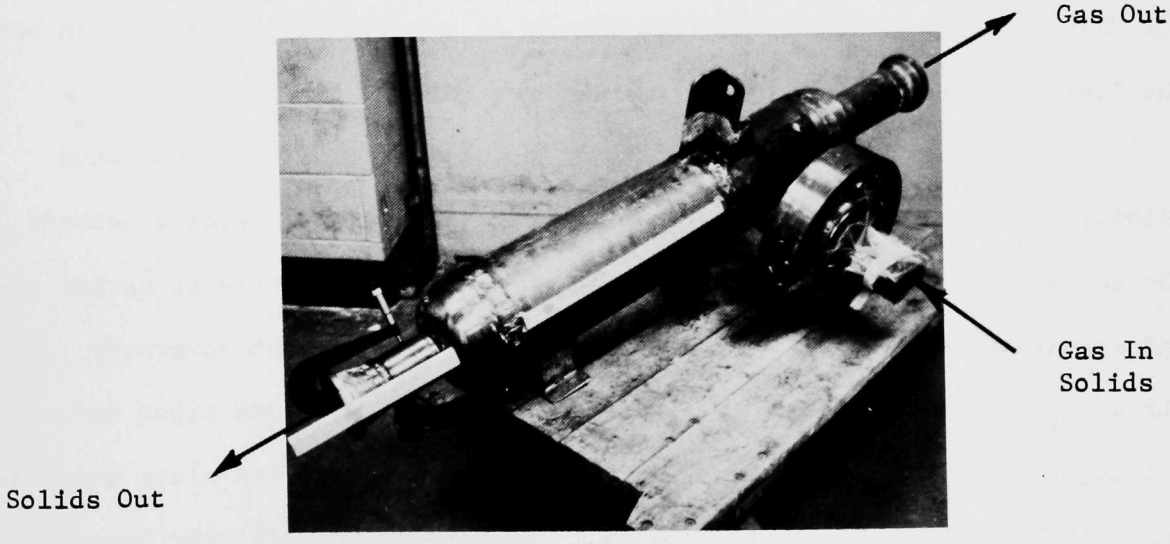

Fig. 14. IGT HYGAS Raw Gas Cyclone. Neg. No. MSD-62449.

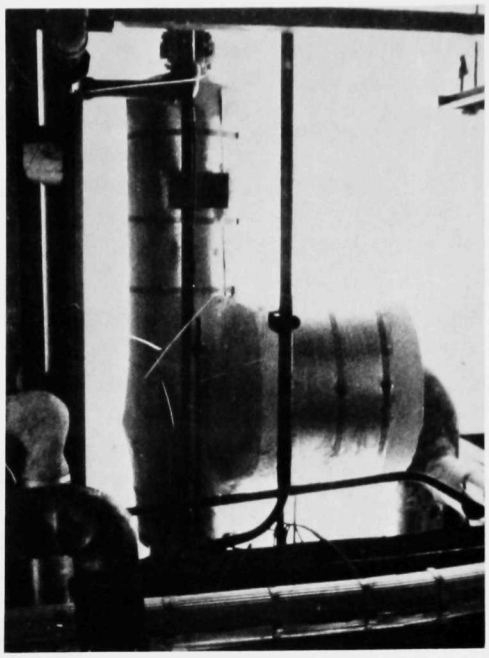

Fig. 15. Raw Gas Cyclone Installed in IGT HYGAS System. Neg. No. MSD-62448.

mapped on the outer surface of the solids outlet neck area. The thickness of the material was ultrasonically measured at each of these points and recorded (Figs. 16 and 17). The cyclone was then reinstalled into the HYGAS system for subsequent operation. The cyclone is to be removed from the system and returned to ANL for further study during a scheduled shutdown in early February. The same points will be reexamined for any erosion that might have occurred during the interim period. At the time the cyclone is in the lab, it will be fitted with nine air-cooled waveguides and ultrasonic transducers. The cyclone will then be reinstalled into the HYGAS system, and real-time monitoring of any additional erosion in both the Stellite-lined area and the unlined area will be performed.

(c) Preliminary investigation in conjunction with Nelson Stud Welding Service of Lorain, Ohio indicates that their stud welding methods may be adaptable for welding air-cooled ultrasonic waveguides to carbon steel and stainless steel pipes and fittings, quickly and without adversely affecting the metallurgical or structural integrity of these pipes and fittings. Three welding methods were observed at the Nelson plant and evaluated for potential field application. The methods were (1) the Drawn Arc method, which is similar to shielded metal arc welding; (2) Capacitive Discharge, which utilizes a large bank of charged capacitors to furnish an

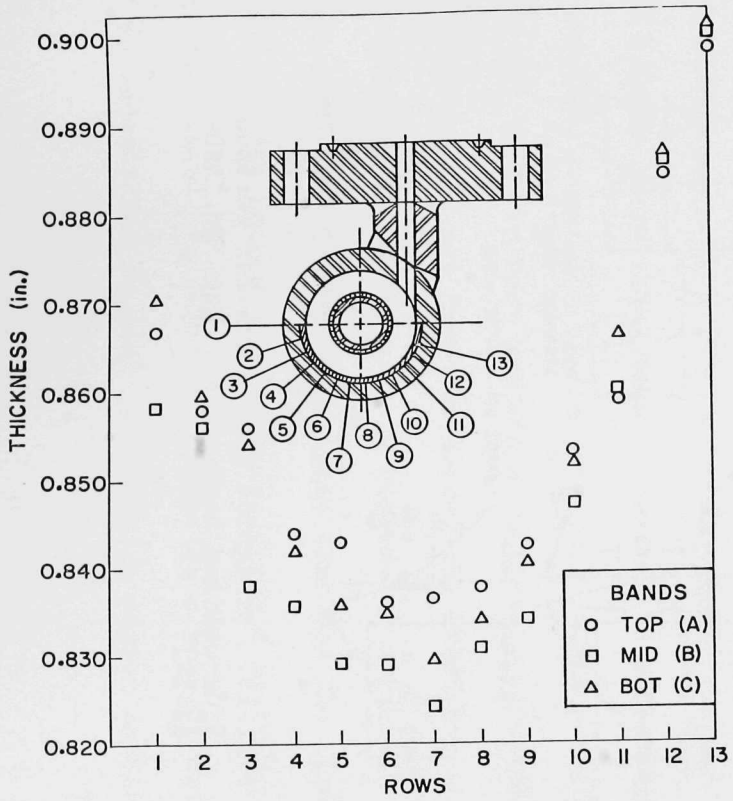

Fig. 16. Graph of Cyclone Wall Thickness in Raw Gas Inlet Area. Neg. No. MSD-62439.

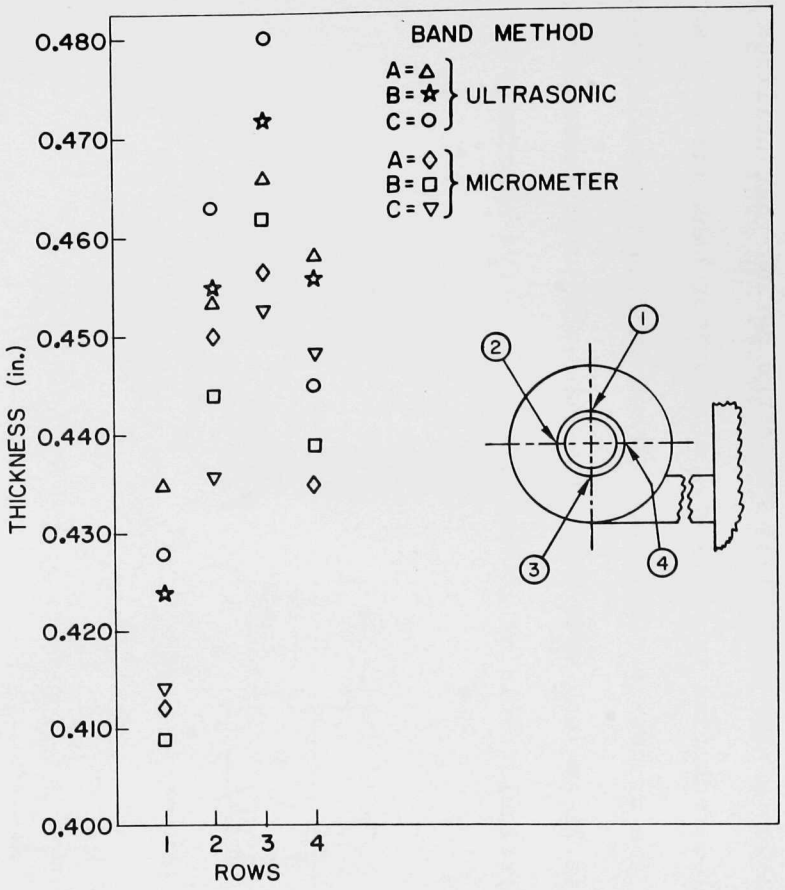

Fig. 17. Graph of Cyclone Wall Thickness in Solids Outlet Neck Area. Neg. No. MSD-62440.

intense current of quite short duration; and (3) the Stored Arc method, which is a variation of the Capacitive Discharge method that utilizes a silicon-controlled rectifier to trigger the capacitor bank and thus more closely control the process parameters. Eleven knurled waveguide specimens 1.59-cm diam x 15.24-cm long were prepared with weld-joint geometries appropriate to the particular welding method (Fig. 18). Five specimens were

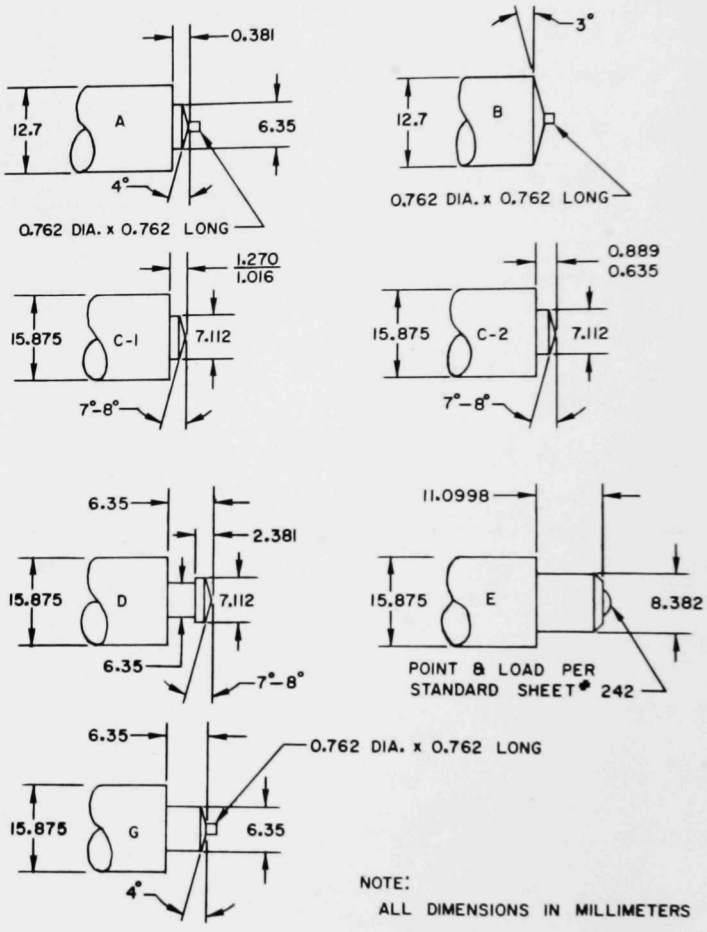

Fig. 18. Waveguide Geometries for Various Stud-welding Techniques. Neg. No. MSD-62434.

welded by the Capacitive Discharge method, four by the Stored Arc method, and two by the Drawn Arc method (Fig. 19). Each weld specimen was ultra-

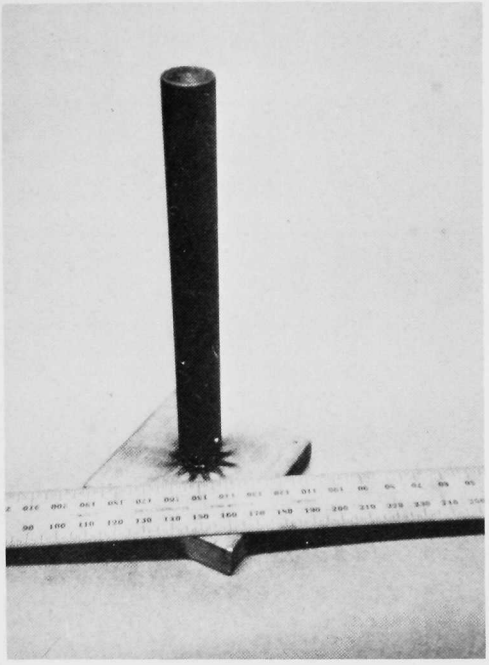

Fig. 19. Waveguide Weld Specimen. Neg. No. MSD-62447.

sonically tested by means of a Branson 303-B pulser-receiver/Aerotech 1.27-cm-diam 5.0-MHz gamma transducer system in the pulse-echo mode to determine the acoustical properties of the weld joint. The results of the test indicate that all three methods produce acoustically acceptable weld joints (Table XI). However, it was observed during the welding procedures that the Stored Arc method was less sensitive to procedural variables such as surface oxide contamination and electrode alignment than was the Capacitive Discharge method. The Drawn Arc method requires considerable melting of the base metal (as does shielded metal arc welding), producing a heat-affected zone (HAZ), which could be undesirable in coal-gasification piping applications.

TABLE XI. Comparison of Acoustic Properties of Stud-welded Waveguides

Geometry Code[a]	Weld Method	Plate Material	Back-wall Echo, dB[b]	Interface Echo, dB[b]	Interface Echo Relative to Back-wall Echo
G	CD[c]	304 SS	64	66	Smaller by 2 dB
A	CD	304 SS	74	72	Larger by 2 dB
A	CD with Detergent	304 SS	86	81	Larger by 5 dB
B	CD	304 SS	81	77	Larger by 4 dB
B	CD with Detergent	304 SS	74	70	Larger by 4 dB
C-1	SA[d]	304 SS	79	63	Larger by 16 dB
C-2	SA	304 SS	78	68	Larger by 10 dB
D	SA	304 SS	68	60	Larger by 8 dB
D	SA	C-1020 Carbon Steel	73	73	Larger by 8 dB
E	DA[e]	304 SS	52	68	Smaller by 16 dB
E	DA	C-1020 Carbon Steel	63	77	Smaller by 14 dB

[a] See Fig. 20.

[b] Gain (in dB) required to achieve a signal display at 50% of cathode-ray tube height.

[c] CD = Capacitive Discharge.

[d] SA = Stored Arc.

[e] DA = Drawn Arc.

Additional developmental work in conjunction with Nelson Stud Welding Service is in progress to optimize the procedures for field welding waveguides to coal-gasification-plant piping and fittings.

(d) A 448-h high-temperature (537°C) ultrasonic amplitude-decay test was conducted using a 1.59-cm-diam x 15.24-cm-long grooved, air-cooled waveguide brazed to a 1.9-cm-thick Type 304 stainless steel block. The waveguide/block assembly was secured across the opening of a 1200-watt Hevi Duty Electrical Company Type 051-PT electrical bench furnace (Fig. 20). A 1.27-

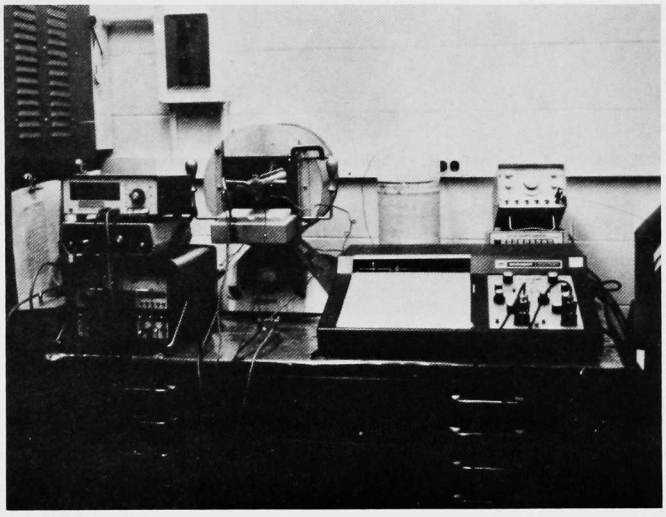

Fig. 20. Air-cooled Waveguide and Furnace for High-temperature Amplitude-decay Test. Neg. No. MSD-62446.

cm-diam 5-MHz Aerotech longitudinal-wave fingertip-contact gamma transducer was mechanically attached to the end of the waveguide using a 0.635-cm-thick disk of neoprene to provide a constant contact pressure. Citgo Premium Lithium Grease No. 2 was used for a couplant. The transducer was connected to a Branson 303-B ultrasonic pulser-receiver fitted with a U-gate plug-in module. The gated analog back-wall-signal output of the 303-B was fed into one channel of a Sargent-Welch two-channel balanced potentiometric strip-chart recorder (Model DSRG). A Chromel versus Alumel thermocouple brazed to

the waveguide near the transducer site was fed into the other channel to record transducer temperature. Another thermocouple brazed to the waveguide/stainless steel block interface area was connected to a Keithly Model 160-B digital voltmeter to measure the interface temperature (Fig. 21). Following an initial 3-h heat-up period the controls were adjusted and the test was begun. The amplitude of the gated back-wall signal decayed by ~64%

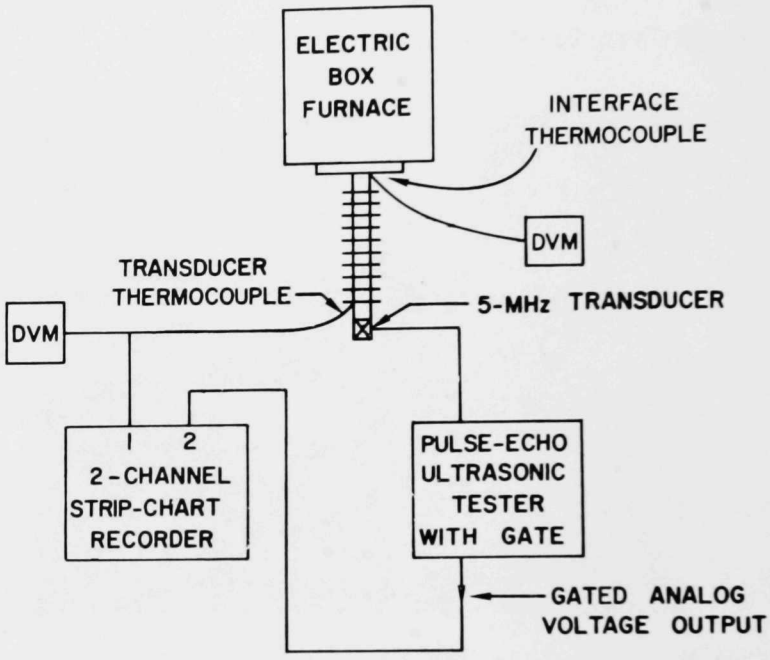

Fig. 21. Instrumentation Block Diagram for High-temperature Amplitude Decay vs Time Test. Neg. No. MSD-62433.

of its original magnitude over the 448-h period, with the largest amount of decay (75%) occurring during the first 170 h of the test (Fig. 22). The gain control on the ultrasonic tester was left at a constant 74 dB during the test with 37-dB gain in reserve, which could have been applied as needed to maintain a constant signal display height. During the 3-h heat-up period, the signal amplitude increased by 500% (14 dB), with a corresponding decrease during the cool-off period following completion of the test. The test

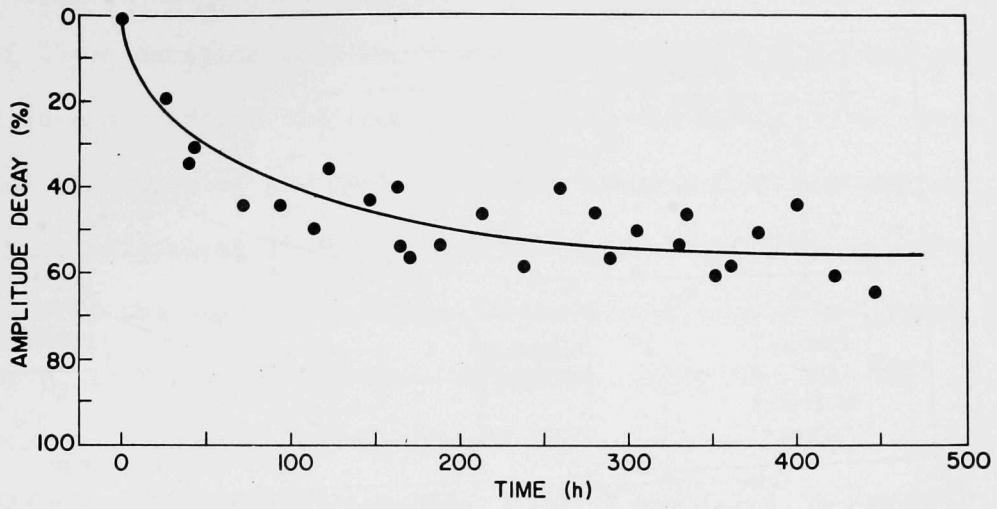

Fig. 22. High-temperature Amplitude Decay vs Time Curve. Neg. No. MSD-62431.

indicates that the transducer signal output is not significantly attenuated by the operating temperatures encountered in the air-cooled waveguide and that the acoustical properties of the materials used in the waveguide are not adversely affected by extended periods at elevated temperatures.

A digital thickness-gauge plug-in module for the Branson 303-B ultrasonic pulser-receiver has recently been delivered. A similar long-term test at elevated temperatures will be conducted to determine the stability of the test equipment in the time domain.

3. Acoustic Emission

a. Refractory Crack Initiation and Propagation Detection. The four-point-bend fixture for acoustic-emission detection of crack initiation in refractories at elevated temperatures has been completed, as has the programmable furnace. Figure 23 is a schematic diagram of the test setup. The setup is currently being checked out to determine noise threshold settings using furnace temperature-time histories.

Specimens have been cut for the four-point-bend studies. These include high-density and low-density refractories.

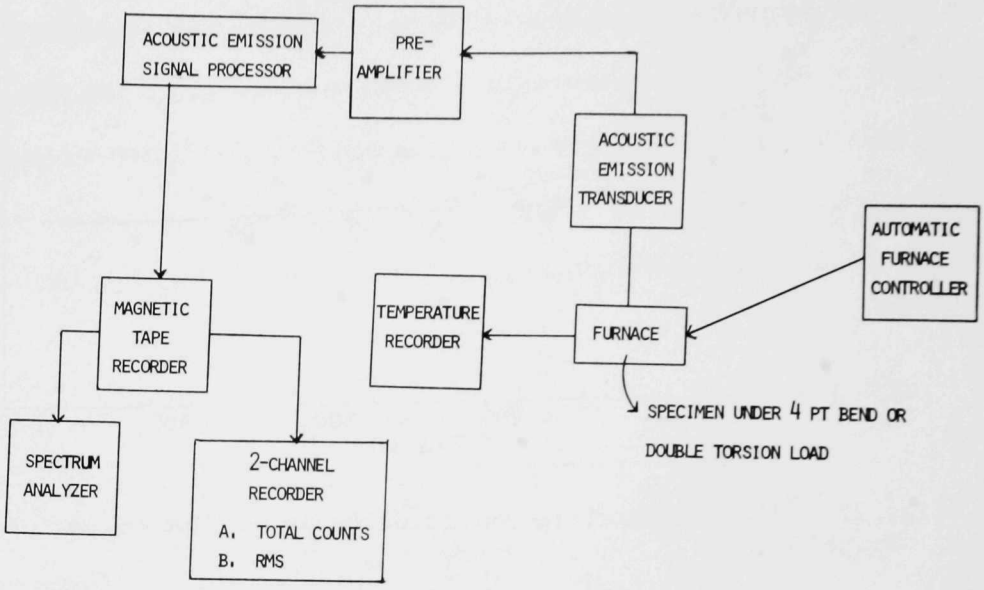

Fig. 23. Schematic Diagram of Acoustic-emission Crack Initiation and Propagation Detection System. Neg. No. MSD-62432.

b. In-situ Valve Leak-detection-system Development. Initial throughflow tests have been conducted on the valve leak-detection system. Figure 24 shows the apparatus and recording system used in the initial flow tests. A fixed cylindrical 1.6-mm-diam orifice was employed to study flow-induced noise. The noise was induced by using differential pressure across the orifice. Three differential pressures (2.04, 2.72, and 5.44 atm) were used on each of three gases (O_2, N_2, and dry air).

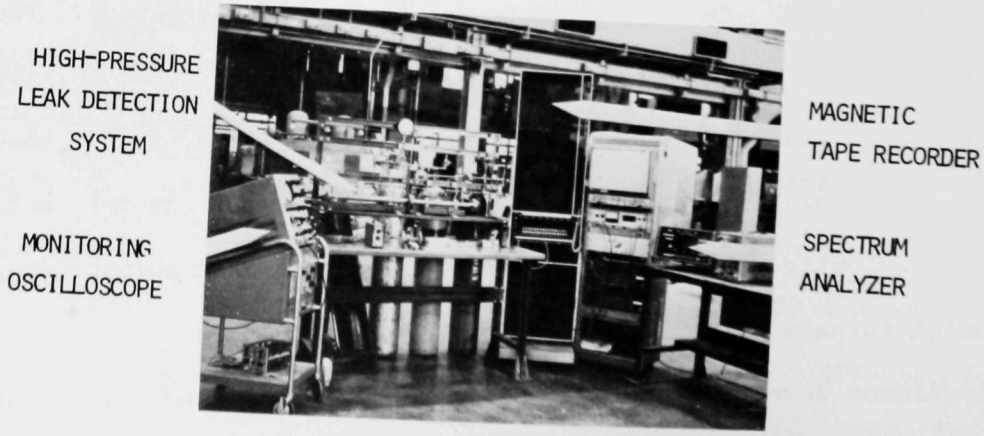

Fig. 24. The 1000-psig Valve Leak-detection System. Neg. No. MSD-62450.

Figures 25a and 25b show spectra of the flow-induced noise for a signal of 25-ms duration from CO_2 flowing through the 1.6-mm-diam orifice with a 2.86-atm pressure differential. Dry N_2 was also used to check the mechanical resonance of the system. Again, using a 2.86-atm pressure differential, a raw signal of 25-ms duration was analyzed in the frequency domain. The results of the spectral analyses of the directly recorded signal are shown for N_2 in Figs. 26a and 26b. Note that, except for the 4320-Hz frequency common to both CO_2 and N_2 flows, their spectral content is significantly different. This indicates that most of the noise was not due to mechanical-component resonance but to flow-induced noise. We will continue this approach with new broad-band transducers and amplifiers.

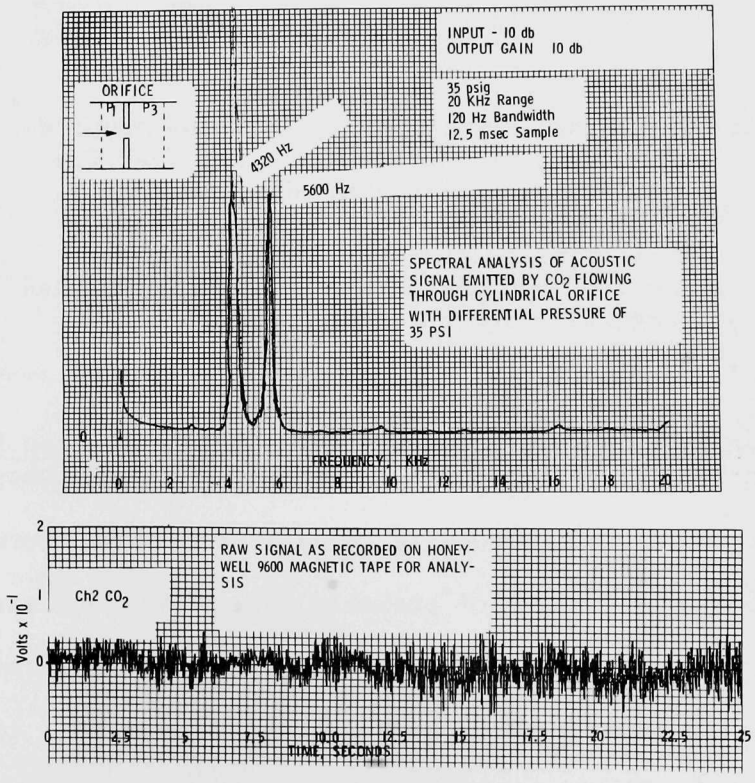

Fig. 25. Accelerometer Output of Flow-induced Noise for CO_2 at Room Temperature. (a) Frequency spectrum of signal obtained from CO_2 flowing through a 1/16-in. orifice with a differential pressure of 35 psig. (b) Example of raw accelerometer signal recorded on magnetic-tape recorder. Neg. No. MSD-62430.

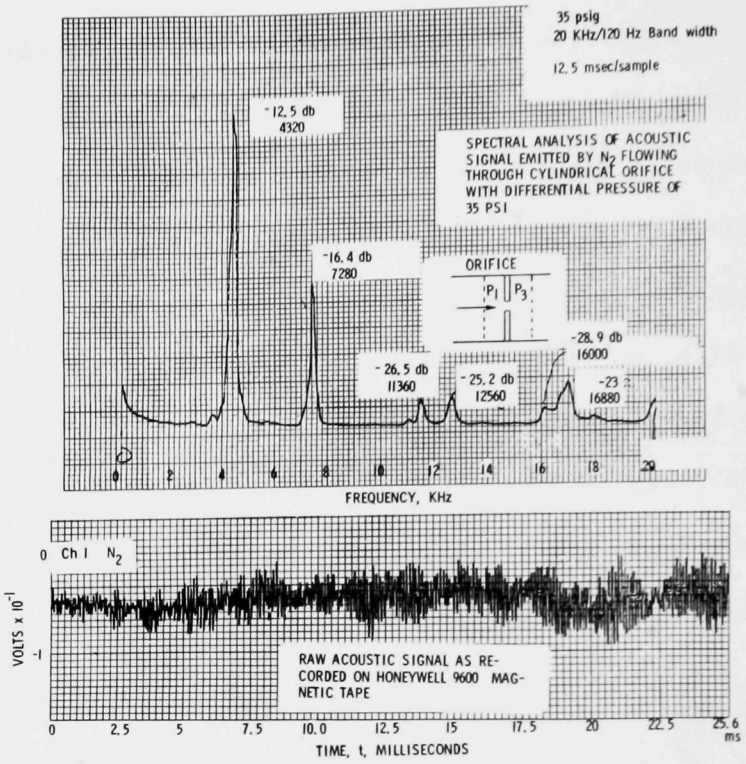

Fig. 26. Accelerometer Output of Flow-induced Noise for N_2 at Room Temperature. (a) Frequency spectrum of signal obtained from N_2 flowing through a 1/16-in. orifice with a differential pressure of 35 psig. (b) Example of raw accelerometer signal recorded on magnetic-tape recorder. Neg. No. MSD-62429.

Task D -- Corrosion Behavior of Materials in Coal-conversion Processes
(Principal Investigators: K. Natesan and O. K. Chopra)

The objective of this subtask is to apply available thermodynamic data and concepts to the prediction of probable corrosion reactions that involve candidate materials over the range of temperatures and gas compositions anticipated in coal-gasification plants. This information, coupled with corrosion-rate data obtained under similar conditions, will be used to select candidate materials for evaluation of mechanical-property changes in simulated gasifier-plant conditions. The gas environments in coal-conversion processes are generally complex multicomponent mixtures, and therefore a quantitative

assessment of the extent and type of interaction between the structural materials and the different environments is difficult. The development of alloys that possess good structural integrity at elevated temperatures and inherent environmental resistance requires a better understanding of the mechanisms of fundamental processes such as oxidation, hot corrosion, sulfidation, carburization, and nitridation as well as the interactions between these processes.

Studies on carburization and oxidation of the iron- and nickel-base alloys are being conducted in binary and quarternary gas environments. The carburization behavior of Inconel 600 and 625, Incoloy 800, and Type 310 stainless steel has been evaluated by exposing 50-mil-thick sheet specimens to CH_4-H_2 gas environments for periods of 100, 500, and 1000 h at 875°C. The composition of the alloys used in the present investigation is listed in Table XII. The carbon activities in these experiments were established

TABLE XII. Composition of Alloys Used in Carburization Studies

Alloy	Concentration, wt%							
	Ni	Cr	Fe	Mo	Mn	Si	C	Other
Inconel 600	76.0	15.5	8.0	-	0.5	0.25	0.017	-
Inconel 625	61.0	21.5	2.5	9.0	0.25	0.25	0.037	0.2 Ti, 0.2Al
Incolcy 800	32.5	21.0	46.0	-	0.75	0.50	0.038	0.38 Ti, 0.38 Al
Type 310 SS	20.5	25.0	Bal[a]	-	2.0	0.50	0.058	-

[a]Bal indicates balance.

by equilibrating high-purity alloys of Fe-18 wt%Cr-8 wt%Ni and Fe-8 wt%Ni in the gas environment, analyzing the materials for carbon, and then using the reported[4] data on the carbon activity-concentration relationship for these

alloys. The carbon activities in these experiments ranged from 0.011 to 0.15 at a temperature of 875°C. The weight-change data and carbon concentrations in the tested specimens are listed in Table XIII. These data show that the values for carbon gain obtained by combustion analysis are in excellent agreement with the measured weight change for all the alloys. The results also show that Inconel 600 was the most resistant to carburization and Inconel 625 was mildly carburizing, whereas the Incoloy 800 and Type 310 stainless steel were heavily carburized over the range of our investigation. The time variation of the weight change and carbon gain shows that up to 500 h the surface reaction and carbide precipitation kinetics probably play a dominant role in the overall process. Therefore, carburization-rate expressions will be developed subsequent to evaluation of the metallurgical structures in the exposed material. Figures 27 through 30 show the carburized structures at different carbon activities for exposure times of 100 and 1000 h for all the alloys investigated. The micrographs indicate that the depth of carbon penetration increases with an increase in either the exposure time or the carbon activity. The results also show that at a given carbon activity the extent of carburization increases with an increase in the chromium content of the alloy. Scanning-electron microscopy and electron-microprobe techniques are used to evaluate the type and distribution of carbides present in the tested specimens. The experiments are being continued at 750 and 1000°C to evaluate the temperature dependence of the carburization process. Correlations for the carburization rate as a function of carbon activity, temperature, and alloy composition will also be obtained.

TABLE XIII. Data on the Carburization of Alloys from Gas-phase Exposure Experiments at 875°C

Alloy	Carbon Activity	Exposure Time, h	Weight Gain per Unit Area, 10^{-3} g/cm^2	Carbon Gain per Unit Area, 10^{3} g/cm^2
Inconel 600	0.151	100	a	-0.064
		500	0.248	0.240
		1000	1.37	1.090
	0.05	100	a	-0.066
		500	a	-0.002
		1000	0.014	0.093
	0.011	100	a	-0.064
		500	a	-0.056
		1000	a	-0.062
Inconel 625	0.151	100	0.186	0.188
		500	0.775	0.802
		1000	3.17	3.854
	0.05	100	0.135	-
		500	0.403	0.408
		1000	1.161	0.949
	0.011	100	0.124	0.094
		500	0.112	0.025
		1000	0.434	0.342
Incoloy 800	0.151	100	0.705	0.714
		500	4.266	4.104
		1000	7.102	9.054
	0.05	100	0.456	0.332
		500	1.508	1.721
		1000	3.398	3.314
	0.011	100	0.236	0.155
		500	0.662	0.543
		1000	1.479	1.435
Type 310 SS	0.151	100	1.414	1.700
		500	5.55	5.081
		1000	9.10	10.990
	0.05	100	0.684	0.636
		500	1.972	1.819
		1000	4.780	5.501
	0.011	100	0.335	0.324
		500	0.673	0.573
		1000	2.536	3.091

[a]Weight change was immeasurably small.

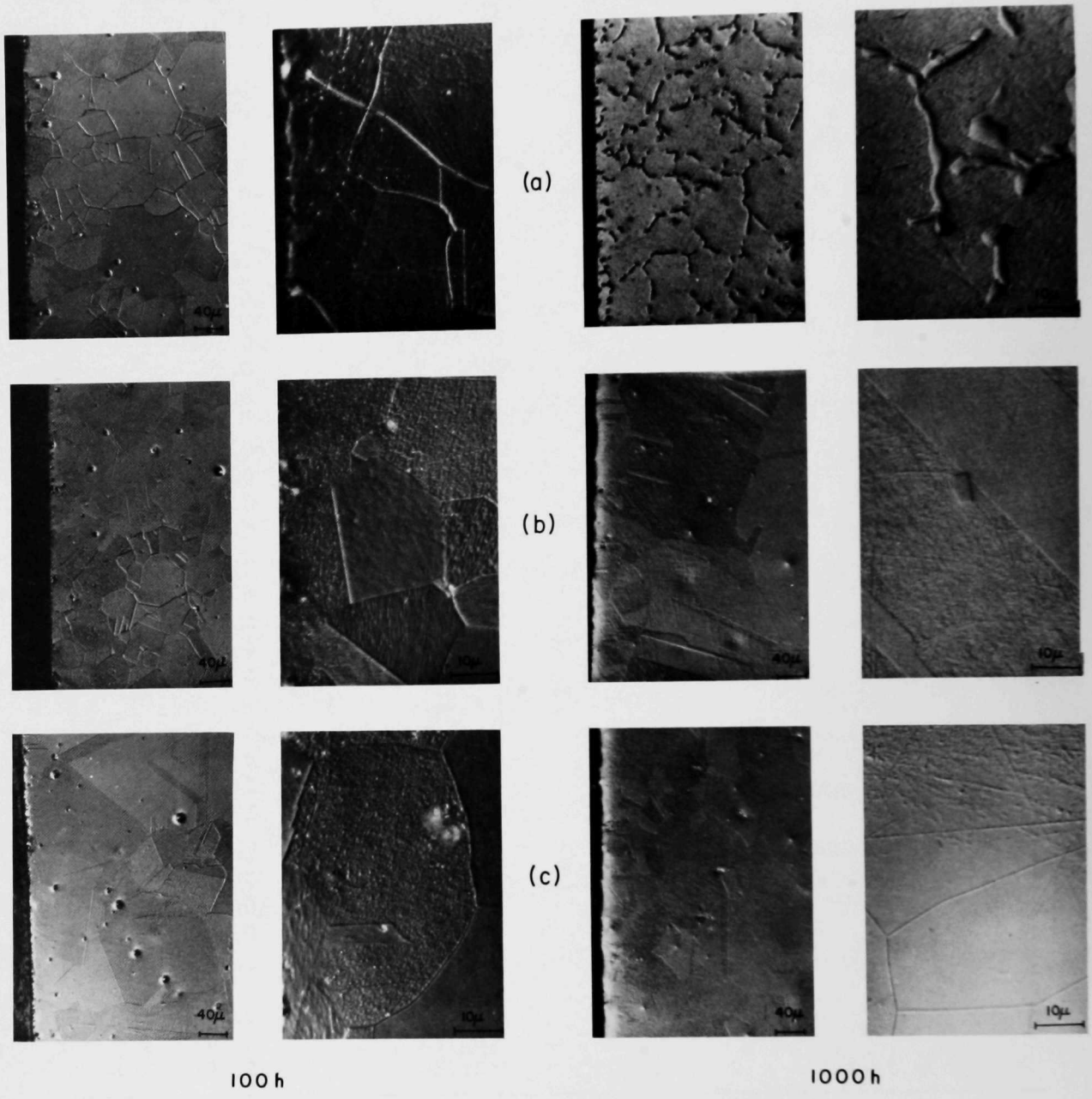

Fig. 27. Optical Micrographs of Inconel 600 upon Exposure to Carburizing Gas Environment for 100 and 1000 h at 875°C. Carbon activities are (a) 0.15, (b) 0.05, and (c) 0.011. Neg. No. MSD-62374.

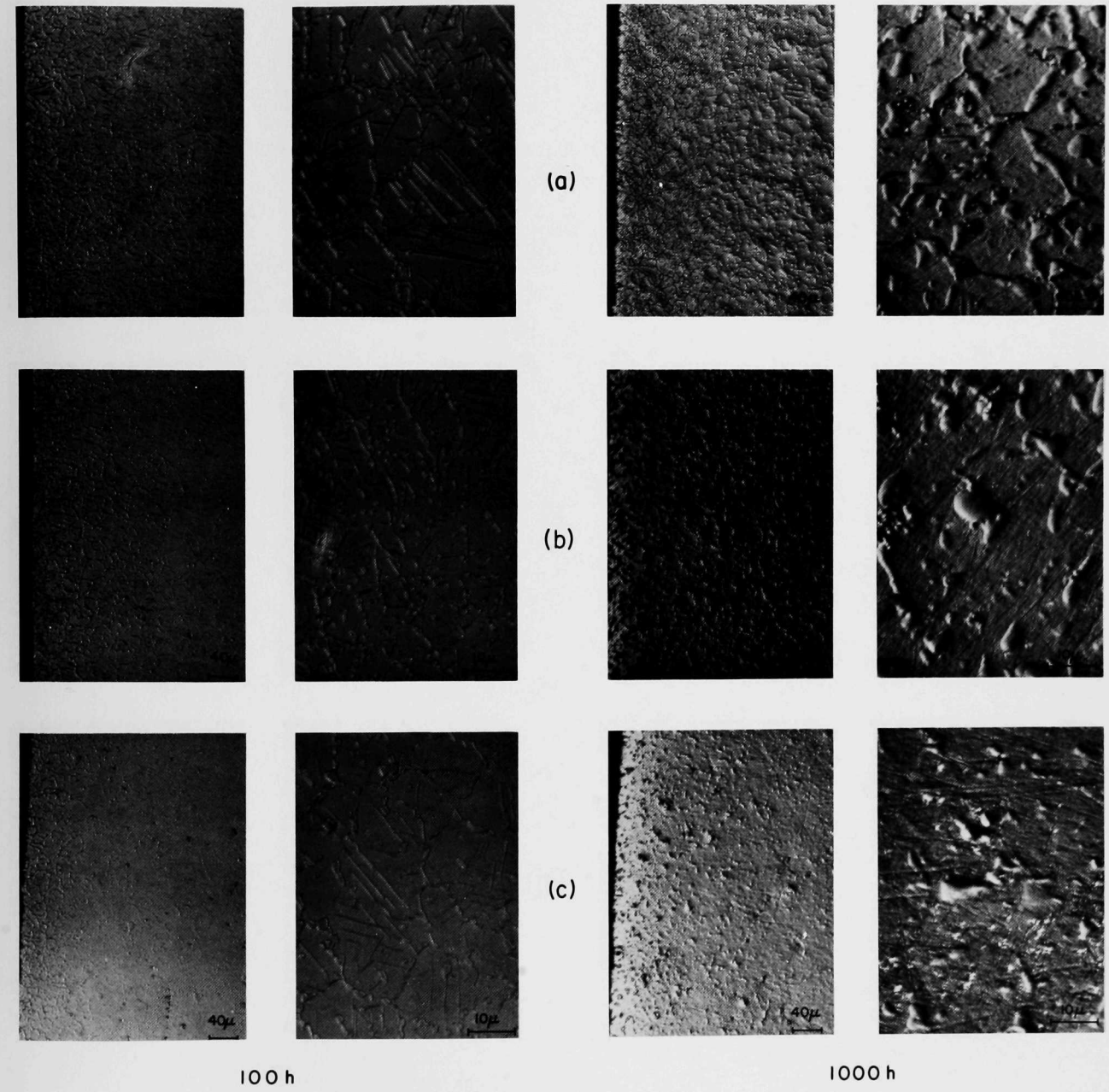

Fig. 28. Optical Micrographs of Inconel 625 upon Exposure to Carburizing Gas Environment for 100 and 1000 h at 875°C. Carbon activities are (a) 0.15, (b) 0.05, and (c) 0.011. Neg. No. MSD-62371.

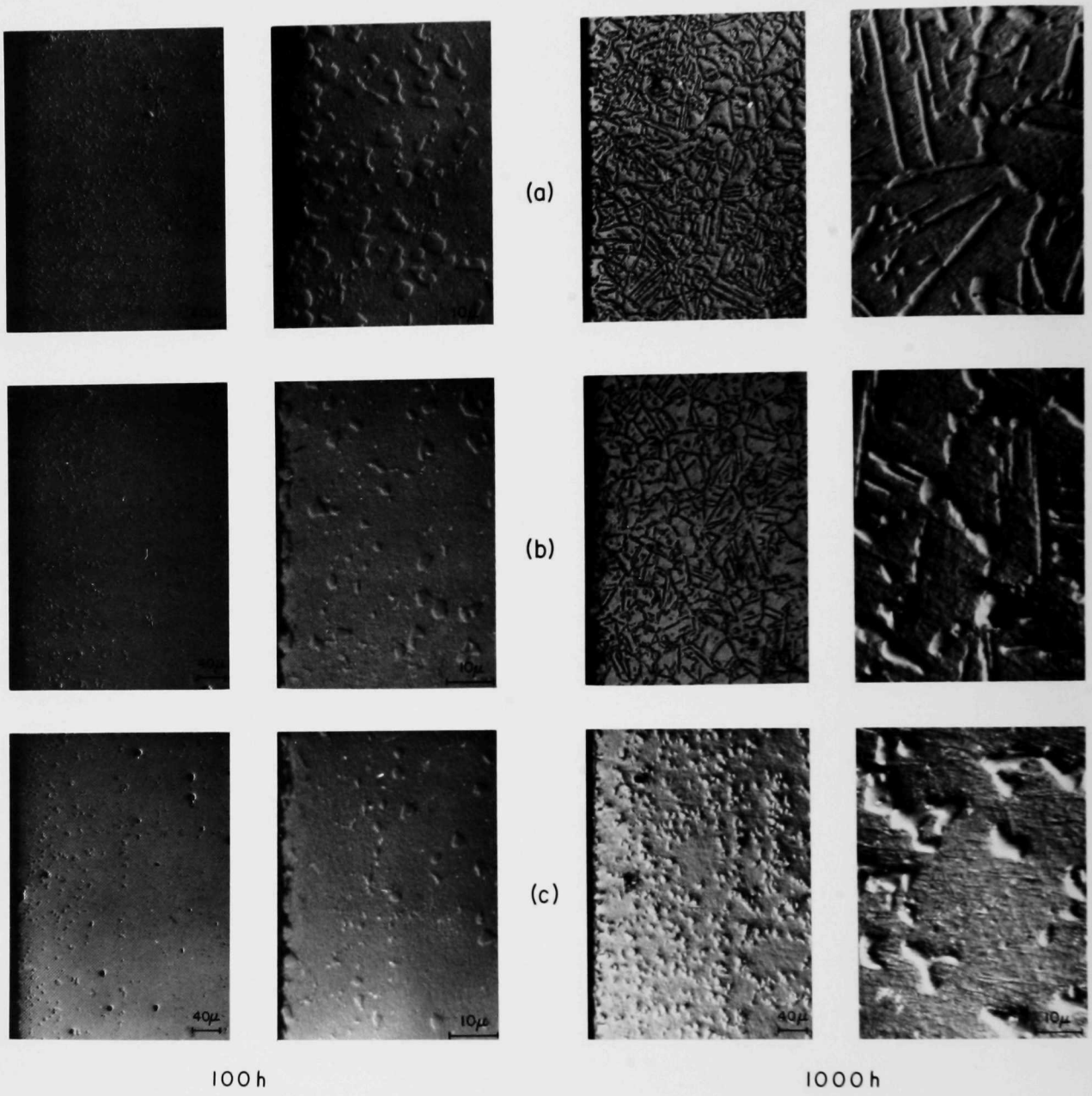

Fig. 29. Optical Micrographs of Incoloy 800 upon Exposure to Carburizing Gas Environment for 100 and 1000 h at 875°C. Carbon activities are (a) 0.15, (b) 0.05, and (c) 0.011. Neg. No. MSD-62373.

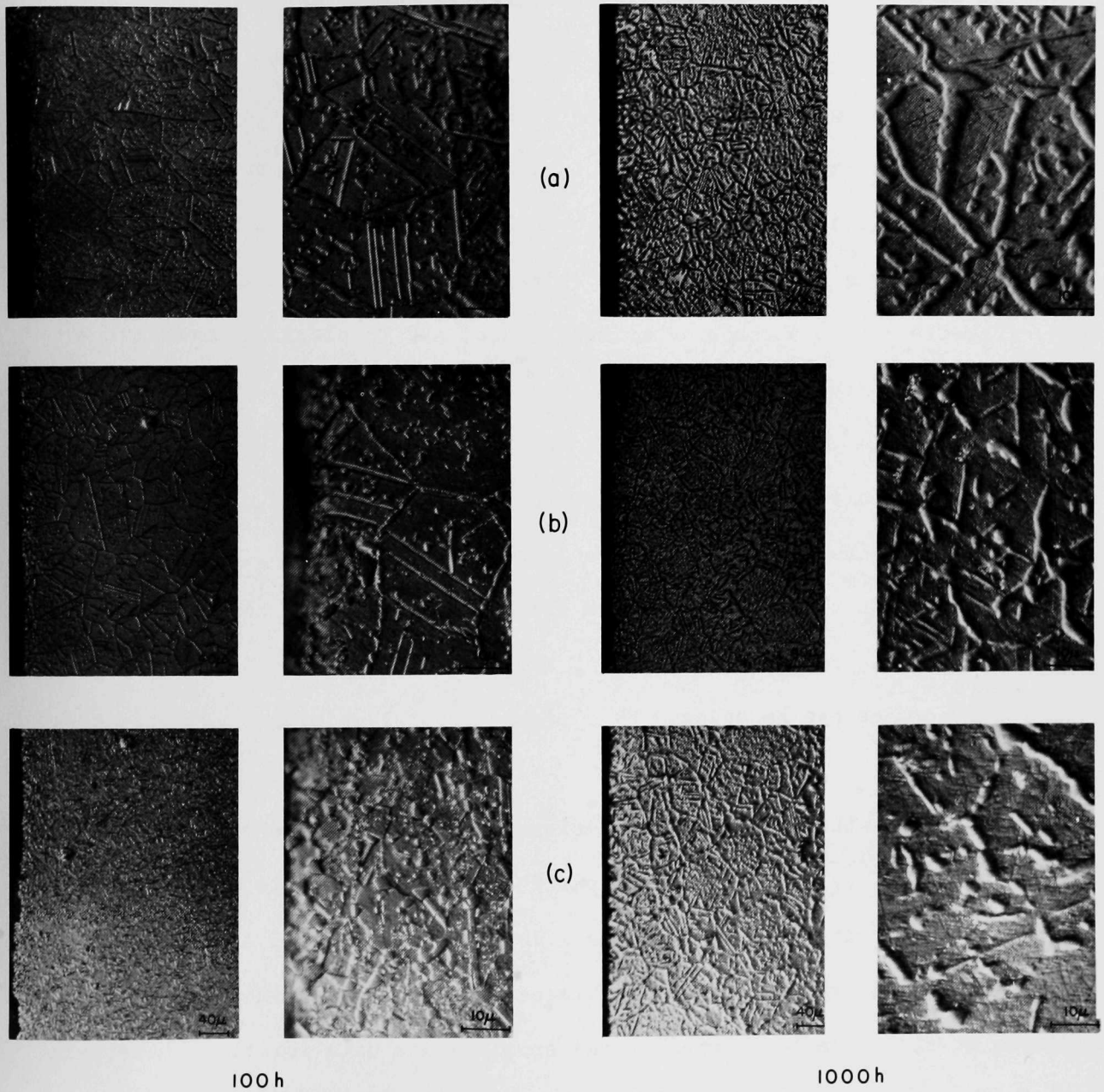

Fig. 30. Optical Micrographs of Type 310 Stainless Steel upon Exposure to Carburizing Gas Environment for 100 and 1000 h at 875°C. Carbon activities are (a) 0.15, (b) 0.05, (c) 0.011. Neg. No. MSD-62372.

Task E -- Erosion Behavior of Materials in Coal-conversion Processes
(Principal Investigator: M. M. Mamoun)

The analytical models developed for determining the material loss by erosion have been extended to take into account the effect of mass flow rate of the erosive media. Considerable effort has been expended to examine the erosion behavior of nominally brittle materials (e.g., refractory ceramics) that are of interest as liners in coal-gasifier vessels. However, to examine the range of validity of the models, numerical erosion rates were computed for materials and conditions for which experimental data exist.

Figures 31 and 32 show experimental data and theoretical predictions for weight loss by erosion as a function of the impact velocity of the eroding particles. Here, W_L^* denotes the ratio of the total weight loss W_L of the eroded surface to the total weight W_1 of the erosive media. Because of collisions between the incoming and rebounding particles, only a fraction of the particles that constitute the erosive media impacts the eroded surface. Thus, the fractional weight of the eroding particles that actually impact a surface can be denoted by Δ_n; experimental evidence indicates that $1/3 \lesssim \Delta_n \lesssim 1/2$.

In Fig. 31 the weight loss experienced by the annealed aluminum surface impacted at 90° by silicon carbide particles (solid line) is proportional to the impact velocity V_i raised to the 2.7 power. The dashed line drawn through the mean values of the experimental points[5-7] has the same slope. Finnie et al.[6] cite some experimental erosion-rate data for these materials at an impact angle of 20°. Since experimental results for the erosion rate of ductile metals at an impact angle of 90° are ∿1/5 of the erosion rate found at 20°, the values given by Finnie were multiplied by 0.2 and designated by the + symbol in the figure.

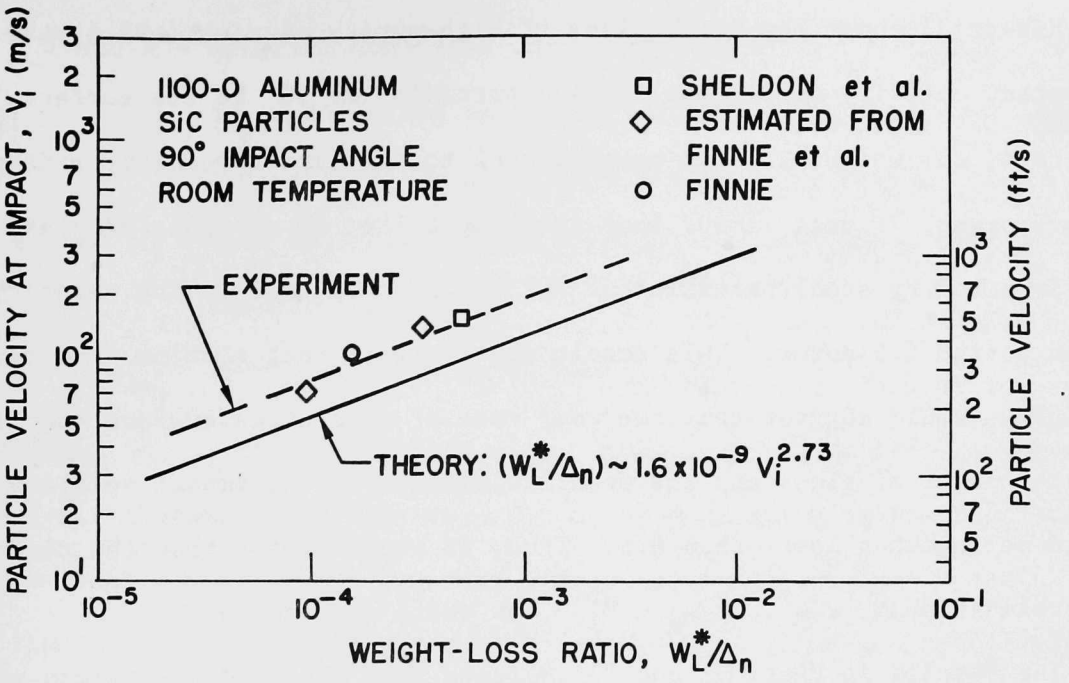

Fig. 31. Comparison of Experimental and Calculated Weight-loss Ratios for an 1100-0 Aluminum Surface as a Function of Impact Velocity of the SiC Particles. The weight-loss ratio W_L^* is the weight loss of the eroded surface divided by the total weight of the erosive media. Neg. No. MSD-62416.

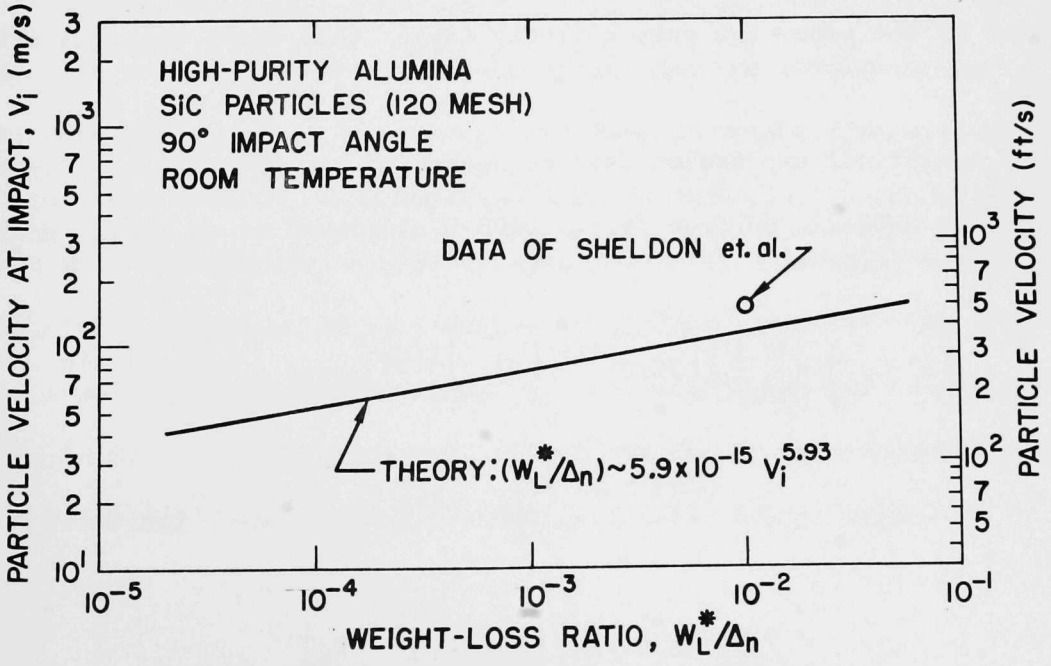

Fig. 32. Calculated Weight-loss Ratio for a High-purity Alumina Surface as a Function of Impact Velocity of the SiC Particles. Neg. No. MSD-62415.

Figure 32 shows the weight loss of high-purity alumina (~99.4 wt%) versus the impact velocity of silicon carbide particles at 90° to the surface. In this case, the weight loss is proportional to the impact velocity raised to the 5.9 power. Finnie[7] found that the weight loss of an annealed glass surface impacted by steel particles at 90° was proportional to the velocity V_i raised to the 6.5 power. This result and the fact that alumina is harder than glass would suggest that the wear rate of an alumina surface should be less than that of glass and the power dependence of the impact velocity should be somewhat lower than 6.5. Thus, it would appear that the theoretical relationship, viz., $W_L^*/\Delta_n \sim V_i^{5.9}$, is quite reasonable.

The results in Figs. 31 and 32 indicate that the theory predicts values that are two or three times greater than those found experimentally for $\Delta_n = 1$. However, as indicated earlier, the experimental data were probably obtained under test conditions in which $1/3 \leq \Delta_n \leq 1/2$. Thus, the values predicted by the model are only slightly larger than those found experimentally.

The analytical expression used to determine the material loss by erosion of a ductile metallic surface (e.g., 1100-0 aluminum) at an impact angle of 90° is

$$\left(W_L^*/\Delta_n\right) = \left[\left(\frac{1}{2}\right)\left(5I/2\right)^{1/k}\left(6/\rho_1\right)^{1/4k}\left(1/p_{fn}\right)^{(4k-1)/4k}\rho_2\, V_i^{(4k-1)/2k}\right], \quad \text{for } V_{ip} \leq V_i \leq V_{ipl}, \tag{1}$$

where

$$V_{ipl} \approx (0.956)\left(p_{fn}/\rho_1\right)^{1/2} D_{uc}^{1.5}, \tag{2}$$

I and k = material constants in the expression $\Delta\varepsilon_p = I\left(N_F\right)^{-k}$, where $\Delta\varepsilon_p$ denotes the plastic strain range and N_F is the number of cycles to failure for completely reversed axial load,

ρ_1 and ρ_2 = mass densities of the eroding particle and eroded surface, respectively, and

p_{fn} = flow stress of the eroded surface.

In deriving Eq. 1, the effects of strain hardening in the material have been neglected. However, when strain-hardening effects are considered, the erosion rates are slightly less than the values obtained from Eq. 1.

The field equations of the linear theory of elasticity, a yield criterion, and various flow rules of the theory of plasticity were used to formulate expressions for (1) the minimum impact velocity V_{ip} required to cause a ductile surface to flow fully plastically under each impact and (2) the size of the elemental volume of material that experiences continuous plastic flow with each impact. An expression for the minimum number of impacts required to cause an element of volume to detach from a given impacted site was derived by postulating that an elemental volume of material detaches when the cumulative plastic strain attains a certain critical value. Finally, Eq. 1 was obtained by integrating appropriately over the eroded surface area. A detailed discussion of the analysis was given previously.[1-3]

The analytical expression derived for the weight loss by erosion of brittle nonmetallic solids (e.g., alumina) at a 90° impact angle is

$$W_L^* = \left\{\left[(3.408)\left(0.105 - 0.243\ B_{eq}\right)^{-1/m_T}\ \rho_2\ \rho_1^{-\left(1+2m_T\right)/5m_T}\ V_i^{\left(6m_T-2\right)/5m_T}\ \Delta_n\right]\Big/\left[N_{F1}\left(1.194\ \tau_{T1}\right)^{-1/m_T}\left(\frac{1-\nu_1^2}{E_1}+\frac{1-\nu_2^2}{E_2}\right)^{-\left(4+3m_T\right)/5m_T}\right]\right\}, \quad (3)$$

for $R_1 > R_{1\ell}$, where

m_T = slope of the stress versus cycles-to-failure diagram (on a log-log scale) for a completely reversed torsional load acting on a material identical to the eroded material $\left(m_T < 0\right)$,

τ_{T1} and N_{F1} = fatigue strength of eroded material in completely reversed torsion at N_{F1} cycles and fatigue life that corresponds to τ_{T1}, respectively, and

B_{eq} = a constant whose value depends on the properties of the eroded surface.

The quantity $R_{1\ell}$, which is the minimum radius of an eroding particle below which the eroded surface experiences microplastic strain, can be computed from

$$R_{1\ell} \approx \left\{\left[(0.607)\ R_c\ E_2\ F_{y2}\right]\Big/\left[\left(1-e_r^2\right)(VHN)\left(\frac{1-\nu_1^2}{E_1}+\frac{1-\nu_2^2}{E_2}\right)^2\right]\right\}, \quad (4)$$

where $R_c \approx 3 \times 10^{-7}$ in. and VHN denotes the Vicker's hardness of the eroded surface. The remaining terms were described previously.[1-3]

The relationship for material loss by erosion of nonmetallic and nominally brittle solids, i.e., Eq. 3, was based on the following. First, the theory of contact stresses (Hertz-Mindlin-Poritsky) of the linear theory of

elasticity was used to determine the stresses, strains, deformation, and maximum pressure that are set up as a result of impact. Next, Auerbach's empirical law and the assumption that the surface of a brittle solid undergoes plastic deformations (microplasticity) if the radius R_1 of the eroding particles was less than a certain lower limiting value $R_{1\ell}$ were employed. Then, for the case when R_1 is greater than some upper limiting value R_{1u}, The Rankine theory was invoked, i.e., fracture of the impacted surface occurs when the largest tensile stress attains a value greater than the ultimate strength of the surface.

These principles and concepts from the theory of fracture mechanics were used to derive expressions for $R_{1\ell}$, R_{1u}, and the minimum velocity V_{ic}, required to cause cracking and fragmentation of the impacted brittle surface. Next, it was assumed that the elemental volume of material that eventually fractures and detaches from a given site is approximately cylindrical, has a surface area equal to the area of contact, and extends to a depth at which the semirange (alternating component) of the orthogonal (to the impacted surface) shear stress attains its largest value. It was also postulated that final fracture and detachment of the elemental volume of material takes place when the shear stress attains a certain critical value. This critical value takes into account the inhibiting effects on crack initiation of the large compressive stress components that arise during impact. By employing all of these concepts and integrating appropriately over the eroded surface area, Eq. 3 was finally obtained.

The minimum mass of Al_2O_3 particles required to cause erosion of an aluminum surface is shown in Fig. 33 as a function of the particle impact velocity. These theoretical results are based on the assumption that $R_e \simeq R_1$ in Eq. 5, where R_e is the average radial distance between any two immediately

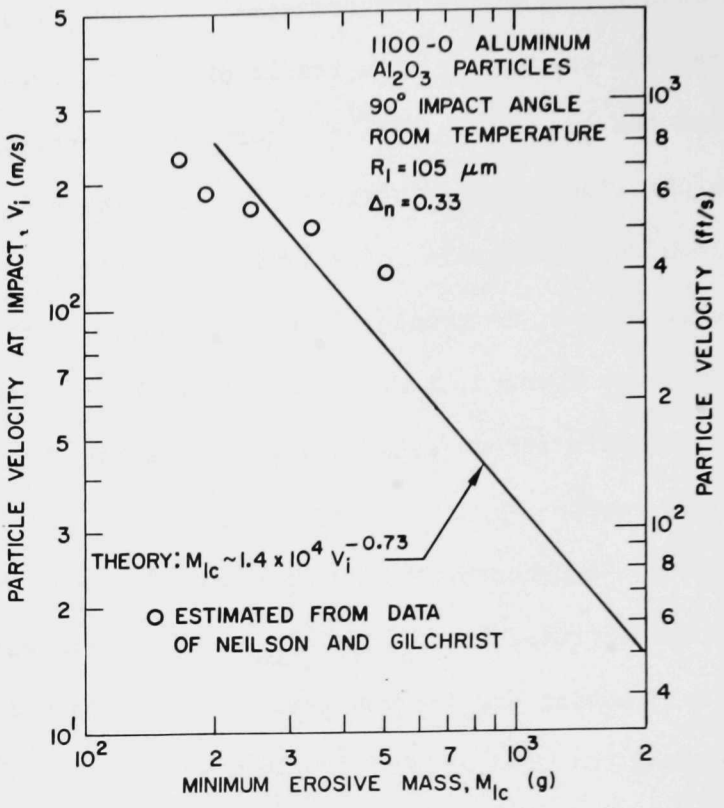

Fig. 33. Comparison of Experimental and Calculated Results for the Minimum Erosive Mass M_{lc} of Al_2O_3 Particles to Cause Erosion of an 1100-O Aluminum Surface as a Function of the Particle Velocity. Neg. No. MSD-62417.

adjacent marks formed on the surface as a result of impact of the eroding particles. The agreement between the predicted values of M_{lc} and those estimated from the experimental data of Neilson and Gilchrist[8] is good in view of the many simplifying approximations.* It is of practical interest to note that no material loss by erosion can occur if the mass of the eroding media is less than a certain minimum value denoted by M_{lc}.

The minimum mass M_{lc} to cause erosion of ductile materials at a 90° impingement angle is given by

---

*It was assumed that the experimental conditions in Ref. 8 resulted in $A_e \simeq 8.0$ in.^{2}, where A_e denotes the eroded surface area.

$$M_{lc} = \left[(4/3)\ (0.4/I)^{1/k} \left(1.5\ \rho_1 / C\ S_{yt2} \right)^{1/4k} \left(V_i/2 \right)^{1/2k} \left(1/\Delta_n \right) \left(R_1^3\ \rho_1\ A_e / R_e^2 \right) \right],$$

for $V_{ip} \leq V_i \leq V_{ipl}$. (5)

The terms C and S_{yt2} were defined previously.[1,2] This relationship is based upon the assumption that fully plastic strains develop as a result of impact and that strain-hardening effects are negligible.

The analytical studies lead to the following general conclusions with regard to the erosion behavior of materials.

1. The average reduction in section thickness of a material by erosion is directly related to the amount of erosive media that impacts the surface.
2. The erosion rate is directly proportional to the mass flow rate of the erosive media.
3. The erosion rate is proportional to the impact velocity of the eroding particles raised to a power between ∿2 and 6, depending upon the properties of the substrate and the eroding media.
4. The effects of strain hardening of the surface on the erosion behavior of a material are small and can be neglected.
5. Materials properties that enhance the erosion resistance of a material are: high values for the flow stress, endurance limit, and yield, tensile, and fatigue strengths and low values for the moduli of elasticity and Poisson's ratio for the substrate and eroding particles.

The above considerations will be useful in evaluating the erosive-wear behavior of materials for various applications in coal-conversion plants. The analytical models can be employed in the early stages of design to ensure

that the requirements of component performance and reliability will be met. Additional experimental data on the erosion behavior of materials of interest, obtained at ANL and other laboratories, will be used to establish the validity of the analytical models and lend greater confidence to the predictions of erosive wear under gasification-plant conditions.

Task F -- Component Performance and Failure Analysis (Principal Investigators: S. Greenberg, D. R. Diercks, W. A. Ellingson, A. Purohit, J. E. Sanecki, W. J. Shack, and J. Y. N. Wang)

1. HYGAS Pilot Plant

a. Instrument Tubes

An abbreviated version of the final report on the failure of the instrument tubes has been distributed. Incoloy 800 tubes, used to replace the original Types 304 and 316 stainless steel tubes in accordance with our recommendation, continue to operate satisfactorily.

b. Coal Pretreatment Vessel Cooler

The coal pretreatment vessel originally contained six coolers (water-to-air fluidized-bed heat exchangers) to control the temperature of the exothermic oxidation reaction. Four were spaced around the periphery of the cylindrical vessel and two were in the center. Heat-transfer calculations indicated that four are adequate, but the two additional coolers were placed in the center to provide greater cooling capacity.

Operation with six coolers apparently resulted in poor temperature distribution. An iron-constantan thermocouple melted, and its Type 316 stainless steel protection tube was severely oxidized. One of the central coolers failed as a result of a central pipe rupture, and many of the other pipes in these coolers were severely bowed.

No evidence of accelerated corrosion or oxidation of the failed cooler is apparent. Stress analysis indicates that failure was caused by

plastic buckling, which probably resulted from excessive cooling of the failed pipe. Metallographic examination of the failed thermocouple protection tube is in progress in an effort to estimate temperatures in various regions of the vessel. (The maximum design temperature is ∿800°F, and the scale of the instrument used to monitor temperature in the vessel only went to 1000°F.)

The vessel is presently operating satisfactorily with four coolers.

c. Start-up Burner Expansion-joint Bellows

The Type 321 stainless steel bellows ruptured as a result of unspecified off-design operating conditions. Metallographic examination revealed that extensive melting had occurred. The pilot-plant operator suspected that coal products had reached the bellows and suggested that we analyze various regions of the bellows for silicon, a suitable "tracer" for coal. Energy-dispersive X-ray and Auger analysis did not indicate any silicon concentrations higher than in unaffected regions of the bellows.

2. Synthane Pilot Plant

a. Process Piping

In cooperation with ERDA-Bruceton, a method of field identification of Synthane plant process pipe--X-ray fluorescence--was designated, and it was agreed to replace carbon steel pipe with the specified materials where process conditions require the replacement. Similarly, it was agreed to measure the hardness of the HAZ of nonspecified $1\frac{1}{4}$ Cr-$\frac{1}{2}$ Mo alloy that contains welded assemblies and replace all alloy components in which the hardness of the HAZ exceeds 200 Brinnell. Repair of the system has been completed.

b. Coal-bucket Elevator

Investigation of the coal-bucket elevator failure was terminated

when it was learned that the appropriate components were not available for examination.

c. Stainless Steel Welded Assembly

This assembly consisted of a Type 316 stainless steel long-radius (shop fabricated) elbow socket welded to a Type 304 stainless steel flange. It was initially reported that the weld had cracked. Metallographic examination also revealed extensive cracking of the pipe and poor welding technique. The crack morphology is indicative of chloride stress-corrosion cracking, and chloride has been detected at various locations in the failed assembly.

It has been concluded that failure of the joint was probably caused by excessive mechanical loading (e.g., as would be produced by reported system modifications after initial installation) of a poor weld and that the chloride (probably introduced with the water used for pressure testing) could have contributed to the extensive cracking observed in the pipe. Because of exposure of the system to chloride-containing water, it is possible that other stainless steel components of the system may also be cracked.

References

1. Materials Science Division Coal Technology Second Quarterly Report, January-March, 1975, Argonne National Laboratory.

2. Materials Science Division Coal Technology Third Quarterly Report, April-June, 1975, Argonne National Laboratory.

3. Materials Science Division Coal Technology Fourth Quarterly Report, July-September, 1975, Argonne National Laboratory, ANL-76-7.

4. K. Natesan and T. F. Kassner, Met. Trans. 4, 2557-2566 (1973).

5. G. L. Sheldon and I. Finnie, "On the Ductile Behavior of Nominally Brittle Materials During Erosive Cutting," Trans. ASME 88B, 387-392 (1966).

6. I. Finnie, J. Wolak, and Y. Kabil, "Erosion of Metals by Solid Particles," J. Materials 2(3), 682-700 (1967).

7. I. Finnie, "An Experimental Study of Erosion," Proc. Soc. for Experimental Stress Analysis, Vol. XVII, No. 2, 1960, pp. 65-70.

8. J. H. Neilson and A. Gilchrist, "Erosion By a Stream of Solid Particles," Wear 2, 111-122 (1968).

ARGONNE NATIONAL LAB WEST
3 4444 00024103 4